UCRL-10932

University of California

Ernest O. Lawrence Radiation Laboratory

SUBSTRUCTURES IN PLASTICALLY DEFORMED COPPER

TWO-WEEK LOAN COPY

This is a Library Circulating Copy
which may be borrowed for two weeks.
For a personal retention copy, call
Tech. Info. Division, Ext. 5545

DISCLAIMER

This document was prepared as an account of work sponsored by the United States Government. While this document is believed to contain correct information, neither the United States Government nor any agency thereof, nor the Regents of the University of California, nor any of their employees, makes any warranty, express or implied, or assumes any legal responsibility for the accuracy, completeness, or usefulness of any information, apparatus, product, or process disclosed, or represents that its use would not infringe privately owned rights. Reference herein to any specific commercial product, process, or service by its trade name, trademark, manufacturer, or otherwise, does not necessarily constitute or imply its endorsement, recommendation, or favoring by the United States Government or any agency thereof, or the Regents of the University of California. The views and opinions of authors expressed herein do not necessarily state or reflect those of the United States Government or any agency thereof or the Regents of the University of California.

Research and Development

UCRL-10932
UC-25 Metals,
Ceramics and Materials
TID 4500 (19th Ed.)

UNIVERSITY OF CALIFORNIA
Lawrence Radiation Laboratory
Berkeley, California

Contract No. W-7405-eng-48

SUBSTRUCTURES IN PLASTICALLY DEFORMED COPPER

Om Johari

M. S. Thesis

September 1963

Reproduced by the Technical Information Division
directly from author's copy

Printed in USA. Price $1.50. Available from the
Office of Technical Services
U. S. Department of Commerce
Washington 25, D.C.

SUBSTRUCTURES IN PLASTICALLY DEFORMED COPPER

Om Johari

Abstract

Transmission electron microscopy techniques were used to study the substructures in single and polycrystals of pure copper deformed under different conditions of static and shock loading. Static loading involved 20% tensile deformation of single and polycrystals at the temperatures 77°K, 196°K and 273°K and strain rates of 1 and 10^{-3} per minute. The shock loading was carried out on thin polycrystalline sheets. The pressures ranged from 16 to 200 kbars.

In tensile deformed specimens no systematic correlation between observed substructure and deformation conditions was found. The substructures varied widely in the same specimen from one region to another. It does not seem possible to correlate changes in cell size to various deformation conditions for two reasons: first, the cells are not always observed, and secondly, there is a wide change in cell size in the areas which show cells. From single crystal observations it was found that at least two slip systems should operate for formation of cells and that the dislocation density is much higher in polycrystals than in single crystals.

In shock loaded specimens the cells were uniform and after a cell size of the order of 0.15 μ, the substructure consisted of microtwinned regions and areas of heavy dislocation density. It was shown that the present theories are not sufficient to specify the exact quantitative conditions for the onset of twinning. It is proposed that this type of analysis should be applied to alloys of different stacking fault energies in order to better understand the twinning phenomenon.

I. INTRODUCTION

A. Tensile Deformation

Transmission electron microscopy has been extensively used to study the substructures resulting from plastic deformation in various face-centered and body-centered cubic metals. Reviews of the various dislocation structures which have been observed have been presented by Swann[1] and Keh and Weissmann.[2] In these reviews various characteristics of cell structure and the factors affecting their size are reported. In polycrystals, plastic deformation causes the breaking up of grains to small, slightly misoriented crystal domains called cells. These cells, consisting of relatively dislocation-free regions are separated by walls containing a high density of dislocations. Warrington[3] has reported that the cell size depends on the temperature of deformation such that an inverse square root relationship between subgrain size and flow stress was obeyed. Cell structures are not observed in metals of low stacking fault energy. In copper, many of the cell walls were parallel to {100} {110} and to a lesser extent to {111}.[3] The complex dislocation arrangements existing in cell walls are often called tangles. However, tangles can also be present without a visible cell structure.

A great deal of transmission electron microscopy has been done on the deformation substructure of Cu single crystals. Howie[4] found that during the second stage of deformation, a non-uniform cell structure was obtained because of ragged dislocation arrangement. He also found that the dislocation density within the cell was about five times smaller than that in the cell wall. It was not possible to resolve slip planes during this stage. Young[5] and Livingston[6] have done some dislocation density calculations using etch pit techniques for copper single crystals. According to Livingston,[6] after sufficient strain the dislocations are distributed in a rough cell structure.

It may be mentioned, however, that the cell structure normally resolved by electron microscopy is not resolved by the etch pit method. Fourie and Murphy[7] have made a study of elongated dislocation loops in the first stage of deformation in copper single crystals. In their work they have proposed a mechanism which leads to hardening in Stage I and brings about transition from Stage I to Stage II.[7] In this model, it is thought that the dislocation loops indirectly act as obstacles to moving screw dislocations. The recent results of Basinski[8] on dislocation arrangements in copper crystals deformed at low temperatures throw more light on the deformation process. From his work and as will be shown later, the geometry of the deformation processes for single crystals fit in very well with the electron microscopy observations. No electron microscope studies have been reported concerning the effect of grain size or rate of deformation on cell formation. It is from this point of view that the present work was undertaken. It was believed that a correlation between cell size and variables like strain rate, grain size, temperature, flow stress and energy of cold work might be found. For this work, two grain sizes--single crystal and polycrystals (70-100 grains/cm), and two strain rates--10^{-3} in/in/min. and 1 in/in/min., and three temperatures--77°K, 196°K and 273°K were selected.

To further study the strain rate effects, some work was also done on explosively deformed copper.

B. Explosive Deformation

No reports of transmission electron microscopic investigations of substructures resulting from explosive deformation have been found in the literature. Nolder and Thomas[9] studied the effects of shock wave propagation in nickel and observed that the cell size decreased with increasing shock pressure until after a critical cell size of $\sim 0.15\ \mu$ was reached the mode

of deformation changed to twinning. This occurred at and above 350 kbar. It was suggested that the pressure required to initiate twinning has to be related to the energy to form twins. In turn, this energy is related to the stacking fault energy. The twin thickness was observed to be <5000 Å and was not detected by previous replication methods, e.g., Glass et al.[10] did not find any twins in their investigations on explosively deformed copper single crystals using x-ray and light optical microscopy. As far as twinning is concerned, Venables[11] has reported that a resolved shear stress of 15 kg/mm^2 ($\approx$ 1.5 kbar) is required to get twinning in the tensile deformed copper single crystals. For example, in copper single crystals deformed in tension, a deformation of 75% or more is required at 4.2°K. Venables[11] reports that the width of the twins to be less than 5000 Å, as was found in explosively deformed nickel.[12]

The study on explosively deformed copper was made to investigate the effects of very high strain rates, and to compare the behavior of copper with nickel[12] in terms of their differences in stacking fault energy (Cu ~ 40 ergs/cm^2, Ni ~ 80 ergs/cm^2).

II. EXPERIMENTAL PROCEDURES

A. Single Crystals

For all tensile deformed specimens copper of 99.999% purity was used. The copper was supplied by United Mineral & Chemical Corporation of New York, U.S.A. and its analysis was:

Iron	- less than 3 parts per million
Silicon	- less than 2 parts per million
Lead, Magnesium, Manganese	each less than 1 part per million
Silver	- less than 2 parts per million

The single crystals were prepared by the moving furnace method using Bridgman's technique. The metal, in the form of a sheet 5" x 5/8" x 1/32", was placed

in a graphite mould. The furnace was maintained under a vacuum of the order of 10^{-4} mm of mercury. The crystals produced were cut to size on a spark cutter so as to give a 2-inch gauge length for the tensile tests on the Instron machine. The width of the specimens was about 0.3". Six crystals were used in this work and Fig. 1 gives their orientation. These crystals, after spark cutting, were annealed in vacuum at cyclic temperatures between 750°-1000°C for 24 hours. Table I describes the deformation conditions for each crystal.

B. Polycrystals

Copper strip was rolled and annealed in steps until finally the thickness was about 0.025". This thickness was used because of ease in handling and to avoid any buckling which might occur during handling of very thin foils. Final annealing gave specimens of grain size 100-150 μ - six of which were used in this work.

C. Tensile Deformation

The tensile deformation was carried out on an Instron machine. A gauge length of 2 inches was used for all deformations. The deformation was carried out at three temperatures: 273°K (obtained by melting ice), 196°K (obtained by mixing dry ice and acetone), and 77°K (obtained by use of liquid nitrogen). The temperature was checked at regular intervals and maintained within 1°. Two strain rates were used: 1 inch per inch per minute and 10^{-3} inch per inch per minute. Before the tensile deformation, the specimen surface was cleaned in a copper chemical polish solution (50% nitric acid, 25% orthophosphoric acid, and 25% acetic acid), and then washed and stored in ethyl alchohol. After deformation, the specimens were prepared for transmission electron microscopy, as described later.

D. Shock Loaded Specimens

Sandia Corporation[13] of New Mexico supplied the explosively deformed copper specimens. These specimens were ACS reagent grade copper, composition

given by Matheson Colman and Bell catalog for CB 323 CX 1920. The thickness of the foils was 0.002". The assembly (Fig. 2) and the procedure for calculation of pressure values (Fig. 3) is described in Appendix 1. Though seven specimens were supplied, only five were used in this work. These were deformed at 16, 28, 100, 150, and 200 kbars pressure.

E. Preparation of Foils

The tensile deformed specimens were first chemically polished in a solution containing 50% nitric acid, 25% acetic acid, and 25% orthophosphoric acid. When the specimens were thin enough they were electropolished using the window technique and a solution of 33% nitric acid and 67% methyl alcohol at -30°C. As the explosively deformed foils were only 0.5" in diameter, they were mounted on another copper sheet with a square hole in the center and then polished to avoid the buckling which would occur if they were held in specimen clamps. The specimens were initially lacquered around all the edges with Lacomit, leaving a portion of the foil bare which was the exterior anode contact. The specimens were then electropolished until perforation occurred. Specimens which were regarded thin enough for electron transmission were carefully cut off by means of a scalpel.

F. Specimen Examination

The foils were examined in a Siemens Elmiskop I-b electron microscope. An electron accelerating voltage of 100 kv and a projector pole piece of 0.77 mm diameter were employed. The selected area diffraction technique was used to determine foil orientations.

III. RESULTS

A. Stress-Strain Curves

The stress-strain curves for the polycrystals are shown in Fig. 4 and 5. It will be seen that for the same strain rate, there is a small increase in flow stress with decreasing temperature. The flow stress increases with decreasing strain rate. This effect is clearly seen for the 196°K and 77°K specimens (Fig. 5). The trend for 273°K (Fig. 4) specimens is opposite, but actually the difference is so small that it may be due to other factors, e.g., a slight difference in grain size. As the higher strain is attained, the curves deviate from linearity, as is often observed.[14] It is also seen from the curves that this effect occurs more rapidly at the slow strain rate, but within the experimental limits there appears to be little or no effect due to the temperature of testing (within the range investigated).

Figures 4 and 5 show the stress-strain curves for single crystals. The orientations of various crystals before the beginning of deformation is shown in Fig. 1. Although the calculation of resolved shear stress-resolved shear strain curve is necessary to make a detailed comparison of the available data, the trend, however, is similar to that pointed out for polycrystals. Since the deformation was given in one step, it was not possible to determine the exact movement of the tensile axis during the process of tensile deformation and so the resolved shear stress and resolved shear strain could not be calculated very accurately. For two of the crystals, using crystallographic relations, the final position of the tensile axis was determined with respect to the foil orientations. This is in good agreement with the electron microscopy observations as will be seen later.

B. Electron Microscope Observations

1. Tensile specimens

The transmission electron micrographs of tensile specimens show various types of dislocation arrangements. Although it was expected that some kind of cell structure would be obtained in all specimens, the accompanying micrographs show that such is not always the case. Taking polycrystals first--Fig. 7 is a typical micrograph showing cell formation at 273°K for a strain rate of 1 per minute. From areas such as those shown it was possible to estimate the cell size. It was seen that there was no predominent texture. This may be because of the mechanical and thermal treatments given to the specimen before the final deformation. In fact, in polycrystalline specimens, so many different foil orientations are obtained that it appears very difficult to assign any particular crystallographic characteristics to these structures. Figure 6 shows a grain boundary for the same specimen. It is interesting to note here that although the cells are observed at areas near the grain boundaries, no obvious dislocation sources were observed at the grain boundary, although there appears to be a high concentration of dislocations along the boundary. The same is true for other grain boundary pictures also, which are shown in Figs. 9, 14 and 17. Thus, the boundary effect is similar for all temperatures and strain rates investigated here. It may also be mentioned that no dislocation pile-ups were observed at these boundaries. At 273°C and a strain rate of 10^{-3} per minute the cell structure is illustrated in Figs. 8 and 9.

The transmission electron micrographs taken from specimens deformed at lower temperature show quite different structures. Figure 10 is a typical cell structure observed at 196°K after a strain rate of 1 per min. However, there were many areas showing a very high dislocation density and extremely small cells, as is shown in Fig. 11 from the same specimen. This makes it

clear that the cell sizes are not uniform and that the dislocation arrangements vary widely from grain to grain in the same specimen. Exactly similar effects are shown in Figs. 12 and 13, which are for specimens deformed at 196°K and 10^{-3} per minute strain rate. The prominent crystallographic directions are marked on the micrographs and it is quite clear that no crystallographic characteristics can be assigned to these dislocation structures.

At a still lower temperature, the trend in structures is similar to those discussed above. Special care was taken to observe any twinning, but it was confirmed without doubt that 20% strain at a strain rate of 1 per minute and a temperature of 77°K produces no twinning. Micrographs 15 and 16 show some characteristics of the structure at this condition. Cells are present in some areas but are not resolved in others which show very heavy dislocation density (Fig. 16). Figure 18 is at 77°K and a strain rate of 10^{-3} per minute and it also shows dense dislocation regions similar to those in Figs. 11, 13 and 16 at other deformation conditions. Figure 19 is an electron micrograph showing a stacking fault in copper. This is from the specimen deformed 20% at 77°K and strain rate of 1 per minute and undoubtedly formed whilst in the microscope. The cell structure is seen in the background.

The electron micrographs from single crystals show such variations in substructure that no quantitative comparison as to the effect of temperature or strain rate could be made. However, they show clearly that the dislocation density for the same strain for single crystal specimens is much less than that for polycrystalline specimens. The accompanying micrographs from six crystals (Figs. 20 to 27) deformed at three different temperatures and two different strain rates show that cell structure is formed only when two independent slip systems operate,(e.g., Figs. 20, 27). It is also interesting to note here that within the range of temperature and strain rate chosen, no <u>systematic</u> variations were observed in substructure (e.g., compare Figs. 24-26

from same specimens). Crystallographic directions are marked on the micrographs and it is seen that the dislocations tend to lie very close to the active glide planes. The operation of second glide planes (duplex slip) gives structures similar to those reported by Basinski.[8] (Fig. 27)

Summary of observations on tensile deformed specimens:

Although it is difficult to obtain quantitative correlations between substructure and testing conditions due to the wide range of substructures within each specimen, the following qualitative effects are apparent.

(1) Cell formation is favored when two or more independent slip systems operate.

(2) Cell size decreases for increasing strain rate.

(3) Cell size decreases for decreasing temperature of testing.

(4) The dislocation density is a function of grain size, being greater in polycrystals than in single crystals. This effect can be understood if boundary sources are operating during plastic flow.

(5) In the case of single crystals, the dislocations tend to lie very close to the glide planes.

2. Explosively deformed specimens

Transmission electron micrographs of specimens after 16kbar pressure revealed a structure of densely tangled dislocations primarily arranged in cell walls enclosing relatively small dislocation-free areas. The average cell diameter for this specimen was found to be 0.23 μ (range 0.15-0.4 μ) and an example of the structure is shown in Fig. 28. The 28 kbar specimen showed interesting effects. In the same specimen, areas with twins (Fig. 30) and areas with cell structure (Fig. 29) are observed. The cell size could not be measured very accurately, but from the few cells which were clear enough

to be measured, a cell diameter of 0.12 μ (in the range 0.06 to 0.2 μ) has been found. Figure 30(a) is an electron micrograph showing twinning in this specimen and Fig. 30(b) is its diffraction pattern. No extra spots arising from twins are present but, as is shown in Figs. 31 and 32, the twin spots of a (001) orientation actually fall on the matrix spots. Hence, the structure consists of twins--a fact which was also confirmed by dark field work.

The results of specimens after 100, 150 and 200 kbar deformation are strikingly similar to those reported by Nolder and Thomas.[9] In these specimens, apart from twinned areas, there were regions which contained a very high density of dislocations. The twinning planes in each of the micrographs are {111}, as confirmed by trace analyses and by contrast-reversal using dark field technique. It was thus possible to identify the spots arising from twinned areas. Figure 33(a) shows twinning in the 100 kbar specimen. Figure 33(b) is its diffraction pattern. The foil has an orientation of $(5\bar{1}0)$ and the twins T_1 and T_2 are respectively $(13\bar{4})$ and $(13\bar{4})$, as shown by the trace analysis in Fig. 34. The spots in Fig. 33, which do not belong to any of the above three orientations, are attributed to double diffraction. This is easily verified by shifting the origin to (002) type spots, viz., (002), (004), $(00\bar{2})$, etc.

From the trace analysis (Fig. 34) and from Fig. 32, it should be noted that there is a possibility of spots from matrix and twin overlapping. This is shown in Fig. 31 for a foil orientation of (001) and in Fig. 37 for a foil orientation of (110). Micrograph 36(a) and its diffraction pattern (Fig. 36(b)) confirms this. Figure 35(a) shows another region from the 100 kbar specimen. From the accompanying diffraction pattern (Fig. 35(b)) it appears that the foil orientation is between (001) and $(5\bar{1}0)$. The streaking of spots in <110> directions and the type of contrast leads to the conclusion that the twins are very thin. Figure 35(a) also shows that the foil has been preferentially

etched at twins during electropolishing. This gives rise to the thickness contours in the micrograph. Figure 38(a) is from a 150 kbar specimen and Fig. 38(b) is its diffraction pattern. The diffraction pattern is similar to Fig. 33(b) and so the analysis of this micrograph is exactly similar to Fig. 33(a). Figure 39(a) is the electron micrograph and Fig. 39(b) is its diffraction pattern from a 200 kbar specimen. Here again, the twin spots and matrix spots overlap (compare with Fig. 30(b)). The areas at the twins have been preferentially attacked giving rise to thickness contours. Since the twins are very thin, streaks are produced along <111>, the projection of which in the (001) orientation gives rise to the appearance of streaks along <110> directions (which are also the traces of twin planes (Fig. 32)).

TABLE I

Crystal No.	Temp. of deformation	Strain rate	Strain
1	196°K	10^{-3} per min.	20%
2	77°K	10^{-3} " "	"
3	273°K	10^{-3} " "	"
4	273°K	1 " "	"
5	196°K	1 " "	"
6	77°K	1 " "	"

TABLE II

Average Cell Size for Polycrystalline Specimens

Temp. of deformation	Strain rate	Average cell size in μ
273°K	1 per min.	0.59
273°K	10^{-3} " "	0.55
196°K	1 " "	0.45
196°K	10^{-3} " "	0.55 (from only two micrographs)
77°K	1 " "	0.41
77°K	10^{-3} " "	0.63

IV. DISCUSSION

A. Tensile Deformation

1. Cell size measurements

From the accompanying micrographs it is quite clear that a statistical estimate of cell size cannot easily be made. There are some regions in every specimen which show cell-free substructure. However, from the various micrographs, an estimate of cell size has been made for polycrystals and is presented in Table II. It is interesting to note that the cell sizes lie in the range of 0.4-0.65 μ for all the polycrystalline specimens. The results of this work are not in agreement with those of Warrington.[3] The cell size changes are so random that no quantitative correlation between cell size and temperature, grain size, strain rate, energy of cold work, or flow stress can be established. In this connection, it should be mentioned that in the present work the specimen thickness was nearly four times that used by Warrington.[3] This change might account for the difference in results. To obtain a finer foil, more rolling is required and no matter how much annealing is given, some rolling texture is retained. This might also be the reason that in the case of polycrystals no specific crystallographic characteristics can be assigned to cell boundaries (wherever cells are present) or to dislocation tangles. On the other hand, in the case of specimens used for explosively deformed specimens, {100} <100> textures were observed preferentially because the starting foil thickness was 0.002 inches.

2. Effect of temperature

The specimens were deformed at three different temperatures. At the lower temperature the tendency to form tangles is more pronounced. From the accompanying micrographs it is quite clear that the dislocation density is so high that an accurate estimate of it cannot be made. It might be concluded that in the temperature range investigated there is not much change

in substructure. In this connection, it should also be mentioned that twinning in copper does not occur at 77°K and 20% strain. In fact, Venables[11] reported that twinning in Cu was only observed after 75% deformation at 4°K.

3. Effect of strain rate

Not much has been reported in the literature on the strain rate effects on substructure. It appears from this work that though there is a change of 1000 times from 10^{-3} per minute to 1 per minute strain rate, there is no systematic change in substructure although the cell size does appear to increase with decreasing strain rate. There is a structural change in explosively deformed metals which will be discussed in the next section.

4. Effect of grain boundaries

The grain boundaries were expected to have either of the following two effects: first, they may act as barriers to dislocation movement, and dislocations may pile up near the boundaries, even causing some boundary deformation, secondly, the grain boundaries may act as sources of dislocations (e.g., as suggested by Fig. 6). To some extent both these effects were observed. The higher density of dislocations in polycrystals compared to single crystals can be attributed to boundary sources.

5. Single crystal deformations

The single crystal micrographs do not show any systematic variations in substructure with change in strain rate or temperature of deformation. The type of structures obtained are similar to those reported, for example, by Basinski.[8] It is seen from Fig. 20 that dislocations lie on two operating glide planes. Some cross slip has also occurred and the tangles which might lead to formation of cell walls are beginning to appear. In Fig. 21 there is only one slip system operating and dislocations lie on this glide plane. These observations may indicate what happens in those polycrystals in which there

is a high dislocation density and tangles. It is quite probable that, e.g., in Fig. 18 the cell wall is in the plane of the foil, and hence does not give a clear picture of the cell structure. This also explains that the phenomenon of cell formation within the specimen is so random that no quantitative relationships can be derived. Depending on the size of a cell and the orientation in which it is viewed, various substructures could be obtained. It is difficult to pin-point these effects more accurately because the cell walls do not lie along well-defined planes. This is possibly why a great scatter in substructures in polycrystals is obtained, and consequently, the effects of various deformation parameters to substructure cannot be correlated quantitatively without ignoring some of the observed features.

B. Explosively Deformed Specimens

From Figs. 28 to 39 it is seen that the cell size decreases with increasing pressure, and after a critical cell size is reached the mode of deformation changes to twinning. The relation between critical cell size and the pressure is quite different for Cu and for Ni,[12] e.g., in the case of nickel, twinning was observed at a pressure of about 350 kbars and 0.15 μ cell size,[12] while in the case of copper, twinning was observed at a pressure of 28 kbars and nearly 0.15 μ cell size. This large difference in pressures causing twins cannot be due to stacking fault energy only, because the stacking fault energy of Ni is ~ 80 ergs/cm^2 and of Cu is ~ 40 ergs/cm^2. However, there are some differences between the experiments done on nickel and copper. The specimen size and shape were also different (for nickel 3-inch diameter slabs, 1/4 inch thick; for copper 0.5 inch diameter, 2 mil. thick sheets). It is not known what type of compressive waves were produced by the different explosive techniques, and what was the wave velocity, i.e., how long it took the wave to travel from one side of the specimen to the other. Considering all these

things, therefore, no quantitative comparison of the two data can be made without error. But this does not exclude the qualitative fact that explosive deformation at higher pressures gives rise to twinning in both these metals. This twinning occurs after a critical cell size is reached. From the results so far obtained it is not possible to conclude that this critical cell size is constant for various metals, or that this depends on stacking fault energy and other properties of the metal.

According to Kuhlmann-Wilsdorf's theory,[15] the stress required to bow out a dislocation of length ℓ and Burger's vector b beyond its critical radius of curvature is given by

$$\tau_{\ell} \cong \frac{Gb}{\ell} \qquad (1)$$

According to the model of Suzuki and Barret,[16] the criterion for twinning is the stress required for movement of the twinning dislocations from a Lomer-Cottrell barrier which must overcome the surface tension of the double stacking fault produced by this movement and the resisting force of the intersecting dislocations. From the equation of the work required to do this, the stress expression comes out to be:[16]

$$\tau_T = \frac{S}{2b_1} + \frac{2T}{\ell b_1} \qquad (2)$$

where S = stacking fault energy

b_1 = Burgers vector of half dislocation $= \frac{a}{\sqrt{6}}$

T = line tension of half dislocation $\approx \frac{Gb_1^2}{2}$

G = rigidity modulus of metal

ℓ = the mean distance between intersecting dislocations.

Equating (1) and (2) to find critical $\underline{\ell}$, the expression comes out to be

$$\frac{S}{2b_1} + \frac{Gb_1}{\underline{\ell}} = \frac{Gb}{\underline{\ell}} \qquad (3)$$

or $$\underline{\ell} = \frac{2G\cdot(b-b_1)\ b_1}{S}$$

taking $G = 4.5 \times 10^{11}$ dynes/cm^2

$S = 40$ ergs/cm^2

$b = 1/2\ [110]$, i.e., $\frac{a}{\sqrt{2}}$

$b_1 = 1/6\ [211]$, i.e., $\frac{a}{\sqrt{6}}$

$a = 3.615 \times 10^{-8}$ cm

Inserting these values in (3), one gets:

$$\underline{\ell} = 0.036\ \mu$$

And now, calculating the value of critical stress from this value of $\underline{\ell}$

$$\tau_T = \frac{Gb}{\underline{\ell}}$$

$$= 3.2 \text{ kbar}$$

But, it was mentioned earlier that twinning occurred in the neighborhood of 28 kbar pressure. The two values differ by a factor of nearly 10.

Since Suzuki's model, Venables[11] has presented another model. In his opinion, twins are not produced by a pair of twinning dislocations moving away from a Lomer-Cottrell barrier but by extended jogs in glissile dislocations which act as sources of twin nuclei. The stress required to produce twinning should be enough to produce an extended stacking fault loop, and this stress must take into account local stress concentration. According to Venables,[11] the critical stress is given by

$$n\ \tau_T = \frac{S}{b_1} + \frac{Gb_1}{2a_o} \qquad (4)$$

where n is a local stress concentration factor of the order of at least 3. and a_o is the radius of the source. At this critical radius stage, the value of $2a_o$ can be taken as equal to $\underline{\ell}$, the length of bowed dislocations. This gives

$$n\ \tau_T = \frac{S}{b_1} + \frac{Gb_1}{\underline{\ell}} \qquad (5)$$

Combining (5) and (1), taking n = 3, and making similar calculations as above, the values obtained are $\underline{\ell} \approx 0.10\ \mu$

and $\tau_T = 1.1$ kbar

Similar calculations for Ni show that if the stress required for twinning is assumed to be the important criterion, its value comes out to be 6.6 kbar according to Suzuki's model and 2.3 kbar according to Venables' model. The actual reported value for twinning in explosively deformed nickel is in the neighborhood of 350 kbar.[12] From the calculation of stress values, it appears that these models do not give good agreement with actual values. However, from this, it cannot be concluded that stress is not the critical factor. In trying to derive the formulae it has been assumed that the length ℓ of the bowing out dislocations is the same as the mean distance between intersecting dislocations leading to formation of twins (in Suzuki's model) and to be equal to the length of leading partial (in Venable's model). These assumptions are not exactly true. At present, there seems to be no correct way to find out how much these two values of ℓ differ from each other. In both twinning models it is the shear stress required to move the dislocations which is calculated. The pressure values used experimentally do not give the value of the shear stress actually acting for the deformation process. Since the specimen is not subjected to changes in dimensions in the two directions normal to the wave front, some other constrains also come into play. This would mean that the shear stress acting is much different from the applied hydrostatic pressure. On the other hand, if there is some way this critical stress for twinning can be calculated, a correlation between the applied pressure and shear stress acting can be found. At present, there are not enough data to do this.

It was proposed by Nolder and Thomas[9,12] that the criterion for twinning is the amount of work done during the deformation. Using this criterion, and equating the value of energy for twinning obtained by taking the stress value from Suzuki's model[16] and strain value of Wilsdorf's theory[15] to the amount

of plastic work calculated from Wilsdorf's theory, an expression for critical $\bar{\ell}$ can be obtained.[12] Following this method then-

$$S < \frac{G}{2\bar{\ell}h}\,[b^2 - b_1{}^2] \text{ in Venables' model}^{12,17}$$

$$\text{and} \quad S < \frac{G}{\bar{\ell}h}\,[b^2 - b_1{}^2] \text{ in Suzuki's model}^{12,16}$$

where S = stacking fault energy of metal

G = rigidity modulus of metal

b and b_1 are the Burger vectors of unit and Shockley partial dislocations respectively, i.e., $b = \frac{a}{\sqrt{2}}$ and $b_1 = \frac{a}{\sqrt{6}}$

$\bar{\ell}$ = average distance between dislocations

h = adjustable parameter of the order of unity.

Using the following values:

$S = 40$ ergs/cm^2

$G = 4.5 \times 10^{11}$ dynes/cm^2

$b^2 = \frac{a^2}{2}$

$b_1{}^2 = \frac{a^2}{6}$

$a = 3.615 \times 10^{-8}$ cm

the value of $h\bar{\ell}$ comes out to be 0.0245 μ (using Venables' model) and 0.049 μ (using Suzuki's model).

From the experimental results, it is known that twinning occurs when the cell size is between 0.1 and 0.2 μ. Taking the critical value for cell size to be 0.15 μ, and using a factor f to correlate cell size d to the average length $\bar{\ell}$ of dislocation in the cell walls, the value of the factor f in the two models is of the order of 1/3 and 1/6 respectively. This value is quite reasonable and is in agreement with the values of f found by Nolder and Thomas.[9] The corresponding energy values can be obtained by using this value of $\bar{\ell}$, and the expression for plastic work obtained by Wilsdorf's work hardening theory[15] giving $E = \frac{K \cdot G \cdot b^2}{2\ell^2}$ where K is a constant nearly equal to 300. The value of energy, by inserting these various values from above, comes

out to be 1.6×10^9 ergs/cm^3 by Suzuki's model[16] and 6.5×10^9 ergs/cm^3 by Venable's model.[17]

In order to obtain energy input required for plastic deformation due to shock loading, the pressure strain curve derived from Hugoniot curve[18] and shown in Fig. 40 is assumed. Integrating the energy expression obtained is

$$E^p_{shock} \approx p \cdot \frac{2}{3} \ \ell n \frac{v}{v_o}$$

Figure 41 is a plot of the p values and energy obtained from the Hugoniot curve and the above expression for energy. From this curve, the corresponding pressure values for the above energy values are between 76 to 165 kbars. This value is about a factor of 3 to 6 larger than the measured value of p.

In view of all the assumptions involved in the calculations and the differences in experimental technique for copper and nickel, the apparent dependence of twinning on energy is not proved. On this energy criterion, twinning occurs when the energy of plastic work is equal to the energy for twinning. In turn, the energy (or critical stress) for twinning is related to the stacking fault energy. So far, the exact dependence of the phenomenon on the stacking fault energy is not known. However, more experiments of the type described in this thesis should prove fruitful.

Finally, some comments can be made regarding the micrographs. The cell size in Fig. 28 (16 kbar) is very uniform. It appears that as the strain rate increases, the cell size drops and so the scatter in cell size is less. In all the twinning micrographs, there are only one or two active twinning planes and the other two do not operate at all. From the overlapping dislocations on twins, it seems that twins were formed during the first passage of the compressive wave, and that the plastic deformation causing appearance of dislocations occurred later. It is also seen that the dislocation density is much smaller near the twinned regions as compared to those where twinning

has not occurred. Since the specimen was polycrystalline, it may be that some grains were orientated more favorably for twinning. In the 200 kbar specimen there are fewer areas free from twins than in specimens deformed at lower pressures. The actual width of the twins is smaller as compared to the projected width on the micrographs. The details within the twins are not clearly resolved in all the specimens, but from Fig. 39 it is seen that twins do show fringe contrast. It also seems that very few twins cross each other; most of them butt against each other where the twins begin to occur on the other plane. Presumably immobile stair rods are formed at the intersection preventing continued propagation of the intersecting twin.

V. CONCLUSIONS

1. The dislocation substructures formed in copper polycrystals varies widely depending on orientation and the previous thermal and mechanical history of the specimen. The same specimen shows so many different structures that no generalizations regarding cell size and its correlation to effect of temperature, stress, or strain rate is possible.

2. Within the range of this work, it is not possible to assign any systematic change in substructure with change in grain size, temperature and strain rate (excluding explosive deformation). However, it is clear that cells do not form unless at least two independent slip systems operate and that for the same conditions the dislocation density is much higher in polycrystals than in single crystals.

3. In explosive deformation, a uniform cell structure is formed unless the pressure is large enough to cause microtwinning.

4. A microtwinning structure has been observed in explosively deformed copper shock loaded to 28 kbar or greater.

5. A stereographic technique has been shown to be a convenient method of solving electron diffraction patterns from twinned crystals. It is found that twins always occur on one or, at the most, two of the {111} planes.

6. At present, the correlation between critical stress or critical strain energy for twinning cannot be exactly determined because of unknown conditions in the shock wave front. However, it appears that a critical cell size of the order of 0.15 μ is attained prior to twinning.

Acknowledgments

The author is deeply indebted to Professor G. Thomas for his personal guidance during the planning, research and evaluation leading to this thesis and to Professor J. Washburn for his interest and helpful discussions. Sandia Corporation of New Mexico deserves special thanks for supplying the explosively deformed specimens. The Lawrence Radiation Laboratory personnel whose auxillary efforts in making the experimental hardware available are greatly appreciated; these include Messrs. L. O. Seaborn, W. R. Goggin, M. J. Kram and F. W. Park. Sincere thanks are due to Miss S. Zuck for her special efforts in typing this thesis. Thanks are extended to the Inorganic Materials Research Division of the Lawrence Radiation Laboratory, under contract to the Atomic Energy Commission, who supported the project.

Appendix 1

Description of Shock Loading Technique and Calculation of Shock Loading Energy Input

In connection with the method of shock loading, the following is quoted from the correspondence with Sandia Corporation:[13]

"The analysis of the system and the specimen configuration follows (diagrams enclosed). It is rather elaborate and contains some assumptions which were necessary to obtain the pressure values. Specimen numbers correspond to the equivalent marked position on the Up - d diagram. The pressures are also given on the same diagram.

"The specimen foils of pure copper were of the following specification: Thickness (original) 0.002"

Composition (ACS reagent grade, composition given by Matheson Colman & Bell Catalog for CB323 CX 1920)

These foils were sealed in a copper envelope and heat treated at 350°F for 15 minutes in a salt bath.

"The specimen foils were shock loaded using the assembly shown in Figure 2. In this manner, several foils could be shock loaded to differing peak pressures simultaneously. A P-16 plane wave generator was used to establish smooth and stable detonation front in a $1\frac{1}{4}$" thick x 2" x 2" composition C pad. Ordinarily, the $1\frac{1}{4}$" thickness of Comp C is more than sufficient to assume an equilibrium reaction zone in the explosion. Therefore, we assume that we may apply equation of state information to the problem. Since the detonation front is essentially a normal compressive impact, the metal interfaces perpendicular to the induced shock wave will not influence its passage provided the fit is tight and interfaces parallel to it will be completely transparent.

. . . . .

"Now the peak pressure experienced by foils placed at various depths may be obtained using the equation of state data for copper (Los Alamos, private communication). The depths used, foil number, and equivalent pressures are shown in Figure 3. Indicated pressures are estimated to be accurate within ±10%; however, the relative differences in pressures will be somewhat more accurate."

It was derived by Nolder[12] that the shock loading energy input at a pressure p is given by:

$$E^{p}_{shock} \approx p \cdot 2/3 \ \ell n \ \frac{v}{v_o}$$

The value of p is obtained from the Hugoniot curve for copper, the relevant portion of which is reproduced in Fig. 40. From this, the energy values can be obtained for various p values which are shown in Fig. 41.

Appendix 2

Study of Twinning from Electron Micrographs by Use of Stereographic Net

During work on twinning it was observed that a comparison of electron micrographs with corresponding standard projections enables the interpretation of diffraction patterns to be carried out very easily. To do this, first the matrix pattern should be indexed on the micrograph. This will give the foil orientation and thus a standard projection can be drawn for that orientation. On this projection the various (111) planes should be drawn. The traces of these planes can be compared to the traces observed on the micrographs in the direction given by the diffraction pattern after allowing for all rotations.* In symmetrical orientations the habit plane cannot be determined uniquely. The poles on one side of these planes should be reflected on the other side. This determines the pole which moves to the center after this reflection and a corresponding standard projection based on this pole is then drawn. This will then give the positions of new spots relative to matrix spots.

This can be explained by the example in Fig. 34. Here, the foil orientation is $(5\bar{1}0)$. A $(5\bar{1}0)$ standard projection is drawn and it shows the position of various poles and the $(1\bar{1}1)$ plane. It is seen that by reflecting about this plane the $(13\bar{4})$ pole moves to the center. This also shows the position of new spots, e.g., (111) going over to (151). By considering distance ratios, then the (333) pole after twinning on $(1\bar{1}1)$ falls on (151). Hence, extra spots corresponding to (111) and (222) will be obtained on the line joining the origin to (151), and spot (333) will coincide with (151). Similarly, spot $(2\bar{2}\bar{1})$ is reflected to $(00\bar{1})$. Hence, again by taking distance

---

* The rotations involved are: 180° due to inversion between diffraction pattern and image and the angular rotation due to changes in magnetic field between diffraction and image positions.

it is seen that the $(00\bar{6})$ and $(4\bar{4}\bar{2})$ spots will overlap and there will be no extra spots on the line joining (000) and $(00\bar{6})$. Similar effects are shown by reflection about the $(1\bar{1}\bar{1})$ plane. This helps determine the planes on which the twins lie with respect to the foil orientation and also the twinning planes can be identified. This is also illustrated in Fig. 32 for an (001) foil and in Fig. 37 for (110) with twinning on (111) plane inclined to the plane of the foil. It is interesting to note that the diffraction patterns from the two compare very well.

In this connection, a useful relation may also be mentioned. In all cubic systems, if (pqr) is the orientation of the foil and $(hk\ell)$ is the twinning plane, then the new orientation (abc) is given by

$$a = \frac{1}{3h}(-hp + 2kq + 2\ell r)$$
$$b = \frac{1}{3k}(2hp - kq + 2\ell r)$$
$$c = \frac{1}{3\ell}(2hp + 2kq - \ell r).$$

Knowing (pqr) and $(hk\ell)$, (abc) can be found and this would directly give the pole moving to the center.

References

1. P. R. Swann, "Dislocation Arrangements in Face-Centered Cubic Metals and Alloys," Electron Microscopy and Strength of Crystals, ed. by G. Thomas and J. Washburn, Interscience Publishers, New York, 1963, pp. 131-183.

2. A. S. Keh and S. Weissmann, "Deformation Substructures in Body-Centered Cubic Metals," Electron Microscopy and Strength of Crystals, ed. by G. Thomas and J. Washburn, Interscience Publishers, New York, 1963, pp. 231-300.

3. D. H. Warrington, "Dislocation Substructures in Polycrystalline Copper," Proceedings of the European Regional Conference of Electron Microscopy, Delft, 1960, pp. 354-357.

4. A. Howie, "Dislocation Arrangements in Deformed Face-Centered Cubic Crystals of Different Stacking Fault Energy," Direct Observations of Imperfections in Crystals, ed. by J. D. Newkirk and J. K. Wernick, Interscience Publishers, New York, 1962, pp. 283-294.

5. F. W. Young, Jr., J. Appl. Phys. 33, 963 (1962).

6. J. D. Livingston, "Dislocation Studies in Copper Using Etch Pits," G. E. Research Laboratory Report no. 62-RL-3173-M, New York, November 1962.

7. J. T. Fourie and R. J. Murphy, Phil. Mag., 7, 1617 (1962).

8. Z. S. Basinski, "Dislocation Arrangements in Copper Single Crystals Deformed at Low Temperatures," Symposium on the Role of Substructure in the Mechanical Behavior of Metals, Technical Document Report no. ASD-TDR-63-324, 1963.

9. R. L. Nolder and G. Thomas, Acta Met. (in press).

10. C. M. Glass, G. L. Moss and S. K. Golaski, "Effect of Explosive Loading on Single Crystals and Polycrystalline Aggregates," Response of Metals to High Velocity Deformation, ed. by P. G. Shewmon and V. F. Zackay, Interscience Publishers, New York, 1961, pp. 115-143.

11. J. A. Venables, to be published in proceedings of AIME Conference on twinning.

12. R. L. Nolder, Ph.D. Thesis, 1963, Lawrence Radiation Laboratory, University of California, Berkeley, California.

13. Sandia Corporation (private communication).

14. A. Seeger, Phil. Mag., 2, 323 (1957).

15. D. Kuhlmann-Wilsdorf, Trans. of AIME, 224, 1047 (1962).

16. H. Suzuki and C. S. Barrett, Acta Met., 6, 156 (1958).

17. J. A. Venables, Phil. Mag., 6, 379 (1961).

18. M. H. Rice, R. G. McQueen and J. M. Walsh, "Compression of Solids by Strong Shock Waves," Solid State Physics, Vol. 6, Academic Press, New York, 1959, pp. 1-69.

Illustrations

Fig. 1 Orientation of single crystal specimens.

Fig. 2 Assembly for shock loading. All measurements are in inches.

Fig. 3 Plot of pressure vs specimen depth.

Fig. 4 Tensile stress-strain curves for 273°K specimens. Slow strain rate = 10^{-3} inch per inch per min. Fast strain rate = 1 inch per inch per min.

Fig. 5 (a) Tensile stress-strain curves for 77°K specimens.
(b) Tensile stress-strain curves for 196°K specimens.

Fig. 6 Electron micrograph of a grain boundary from a polycrystal pulled 20% at 273°K and 1 per min. strain rate. Both sides of boundary have (110) orientation, but they are tilted with respect to each other.

Fig. 7 Electron micrograph showing cell structure in the same specimen as in Fig. 6.

Fig. 8 Electron micrograph showing cell structure in polycrystal after 20% tensile deformation at 273°K, and 10^{-3} per min. strain rate.

Fig. 9 Electron micrograph showing grain boundary effects in same specimen as above. The foil orientation on the side showing cells is ~ $(10\bar{3})$.

Fig. 10 Electron micrograph showing cell structure in polycrystals after 20% deformation at 196°K and strain rate of 1 per min. The foil orientation is approximately $(\bar{1}12)$.

Fig. 11 Electron micrograph of same specimen as in Fig. 10. The foil orientation is nearly (510).

Fig. 12 Electron micrograph showing cell structure in polycrystal after 20% deformation at 196°K and 10^{-3} per min. strain rate. The foil orientation is nearly $(\bar{1}10)$.

Fig. 13 Electron micrograph showing dense dislocations in the same specimens as in Fig. 12. The foil orientation is nearly $(\bar{1}10)$.

Fig. 14 Electron micrographs showing grain boundary effect in same specimens as in Fig. 12 and 13.

Fig. 15 Electron micrograph showing cell structure in polycrystal after 20% deformation at 77°K and 1 per min. fast rate. The foil orientation is (001).

Fig. 16 Electron micrograph showing dense dislocation region in same specimen as in Fig. 15. The foil orientation is (001).

Fig. 17 Electron micrograph showing grain boundary effects in same specimen as in Fig. 15 and 16.

Fig. 18 Electron micrograph showing dislocation structure in polycrystals after 20% deformation at 77°K and 10^{-3} per min. strain rate. The foil orientation is $(\bar{1}10)$.

Fig. 19 Electron micrograph of the same specimen as in Fig. 15 showing cell structure and deformation stacking fault. The foil orientation is $(\bar{1}10)$.

Fig. 20 Electron micrograph from single crystal deformed 20% at 273°K and 1 per min. strain rate. The foil orientation is nearly $(\bar{1}10)$ and the dislocations tend to lie on one glide plane.

Fig. 21 Electron micrograph from single crystal deformed 20% at 273°K and 10^{-3} per min. strain rate. The dislocations again tend to lie nearly on one glide plane.

Fig. 22 Electron micrograph from single crystal deformed 20% at 196°K and 1 per min. strain rate. The dislocations are lying preferentially on one glide plane.

Fig. 23 Electron micrographs from single crystal deformed 20% at 196°K and 10^{-3} strain rate. The foil orientation is (001).

Fig. 24 The electron micrograph from single crystal 20% deformed at 77°K and strain rate of 1 per min.

Fig. 25 Electron micrograph showing a different area from same specimen as in Fig. 24.

Fig. 26 Electron micrograph showing another area from same specimen as in Fig. 24 and 25.

Fig. 27 Electron micrograph from single crystal 20% deformed at 77°K and strain rate of 10^{-3} per min. The dislocations are lying on two glide planes, the crystal was favorable for duplex slip to occur.

Fig. 28 Electron micrograph from 16 kbar explosively deformed specimens. The uniform cell structure is seen and the orientation is (001).

Fig. 29 Electron micrograph showing dense dislocations as seen in 28 kbar specimens.

Fig. 30(a) Electron micrograph showing twins as observed in 28 kbar specimen. The twins lie on traces of {111} planes along <110> directions. The foil orientation is (001).

30(b) Diffraction pattern from micrograph 30(a), shows no extra spots due to twinning.

Fig. 31 Expected diffraction pattern by twinning on (001) orientation. No extra spots appear and the spots from twinned material overlap those from matrix.

Fig. 32 Stereogram showing movement of poles by twinning on two {111} planes in (001) orientation.

Fig. 33(a) Electron micrograph showing twins in explosively deformed specimen at 100 kbars.

33(b) Diffraction pattern from micrograph 33(a) with foil orientation $(5\bar{1}0)$.

Fig. 34 Stereographic analysis of twinning on $(5\bar{1}0)$ orientation.

Fig. 35(a) Electron micrograph from another region of same specimen as in Fig. 33 showing thickness contrast. The twins have been preferentially etched.

35(b) Diffraction pattern of micrograph 35(a). Streaking in <110> direction is due to twins being very thin.

Fig. 36(a) Electron micrograph from same specimen as in Fig. 33 and 35. The twinning is (110) orientation.

36(b) Diffraction pattern of micrograph 36(a) showing no extra spots due to twinning.

Fig. 37 Stereographic analysis of diffraction pattern in Fig. 36.

Fig. 38(a) Electron micrograph from explosively deformed specimen at 150 kbar The micrograph shows dense dislocations lying away from twins.

38(b) Diffraction pattern of micrograph 38(a).

Fig. 39(a) Electron micrograph showing twin structure in explosively deformed specimen at 200 kbar pressure. Note the fringe contrast at twin interfaces, the high dislocation density in areas away from twins and preferential etching of twinned material. The foil orientation is (001) and the twins are on {111} planes and appear as traces in <110> directions.

39(b) Diffraction pattern corresponding to micrograph 39(a).

Fig. 40 Hugoniot curve for copper.

Fig. 41 Calculated energy vs pressure curve for copper from Hugoniot curve in Fig. 40.

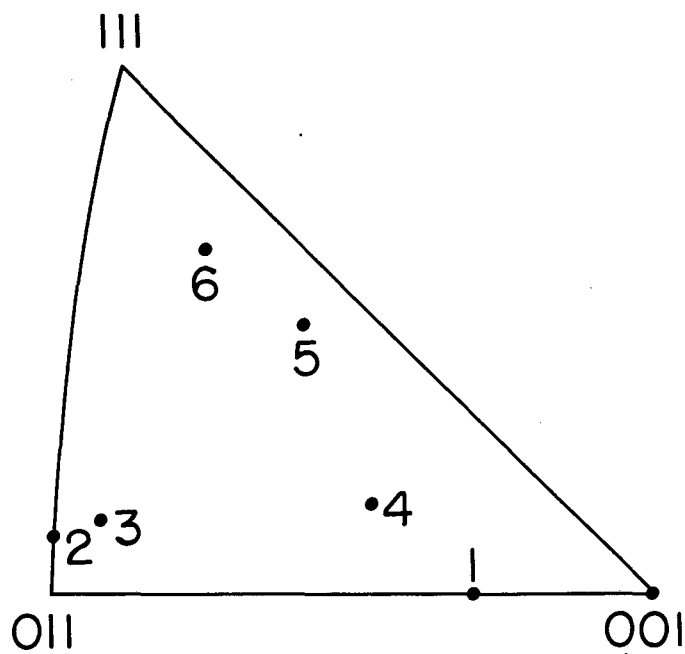

MU-31429

Fig. 1

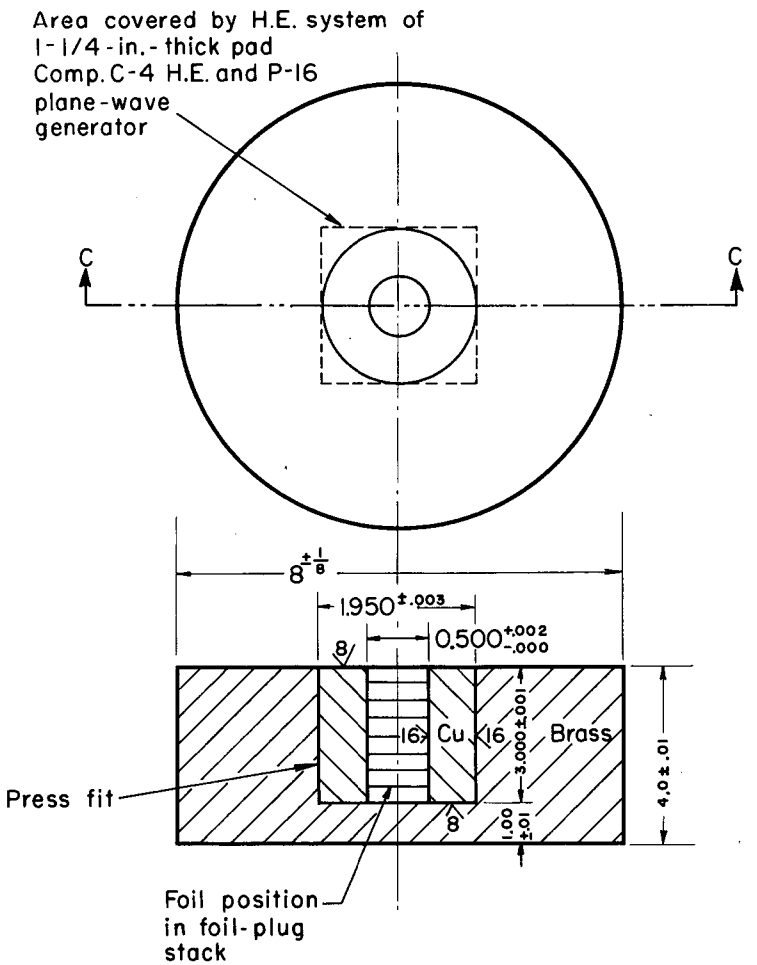
Area covered by H.E. system of
1-1/4-in.-thick pad
Comp. C-4 H.E. and P-16
plane-wave
generator
C
C
8 ±1/8
1.950 ±.003
0.500 +.002 -.000
8
16
Cu
16
Brass
3.000 ±.001
4.0 ±.01
1.00 ±.01
8
Press fit
Foil position
in foil-plug
stack
MU-31430

Fig. 2

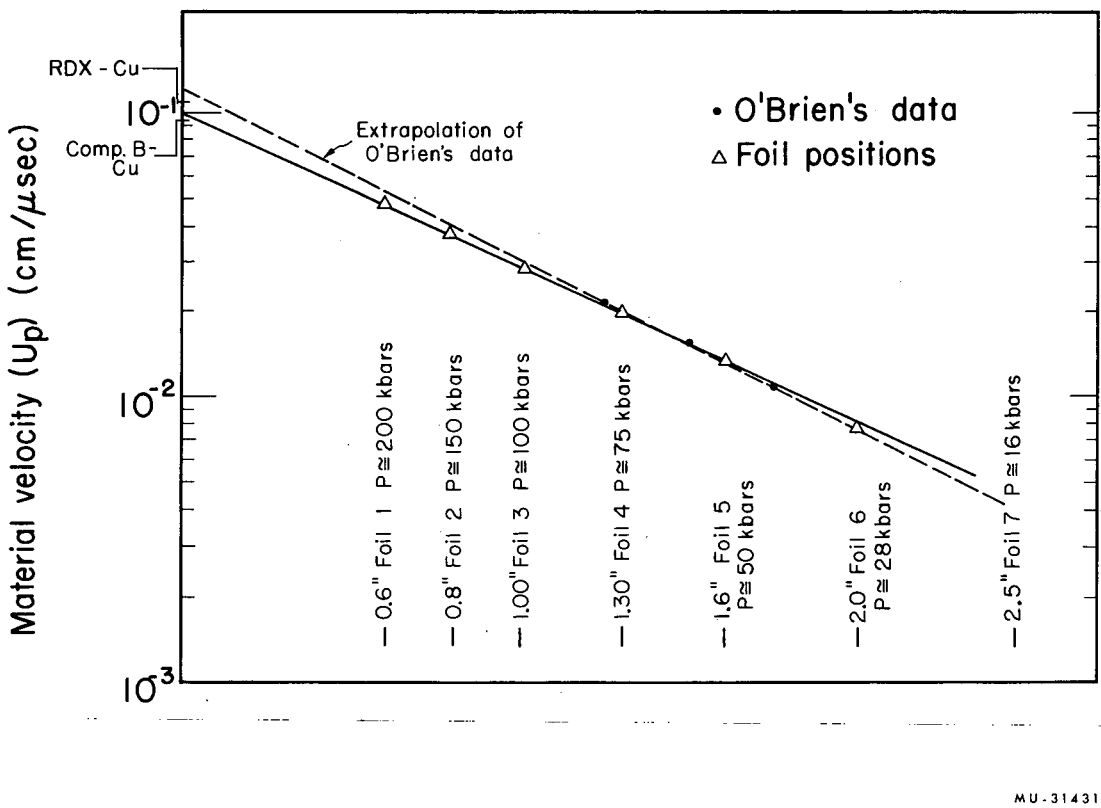
RDX - Cu
Comp. B-Cu
10^{-1}
10^{-2}
10^{-3}
Material velocity (U_p) (cm/μsec)
Extrapolation of O'Brien's data
• O'Brien's data
△ Foil positions
0.6" Foil 1 P≅200 kbars
0.8" Foil 2 P≅150 kbars
1.00" Foil 3 P≅100 kbars
1.30" Foil 4 P≅75 kbars
1.6" Foil 5 P≅50 kbars
2.0" Foil 6 P≅28 kbars
2.5" Foil 7 P≅16 kbars
MU-31431

Fig. 3

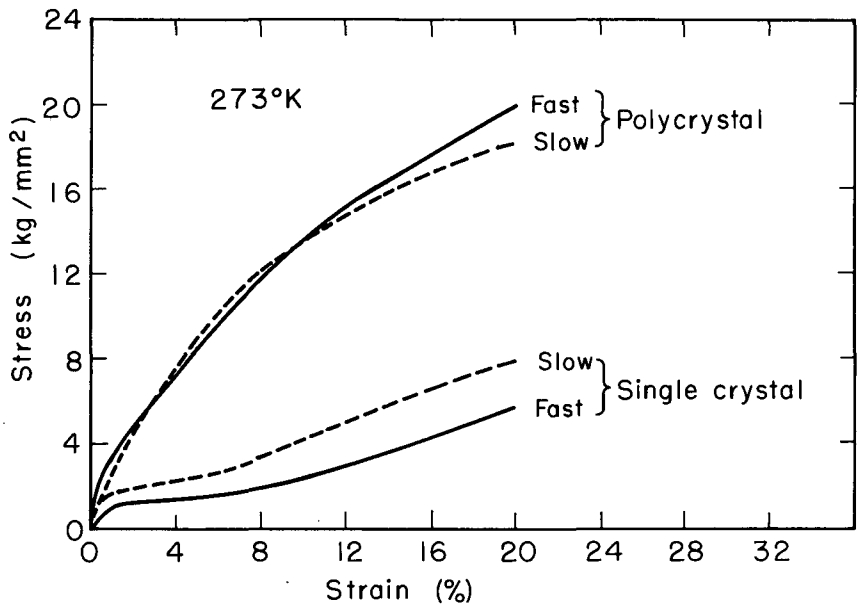

MU-31432

Fig. 4

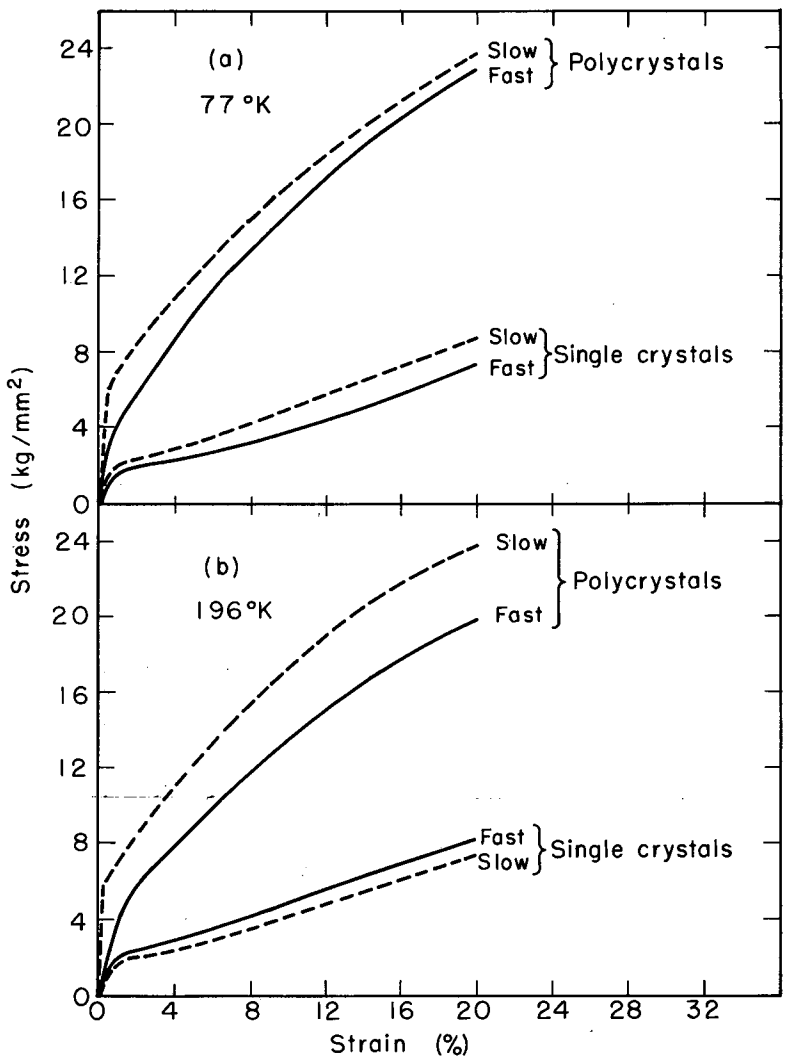

MU-31433

Fig. 5

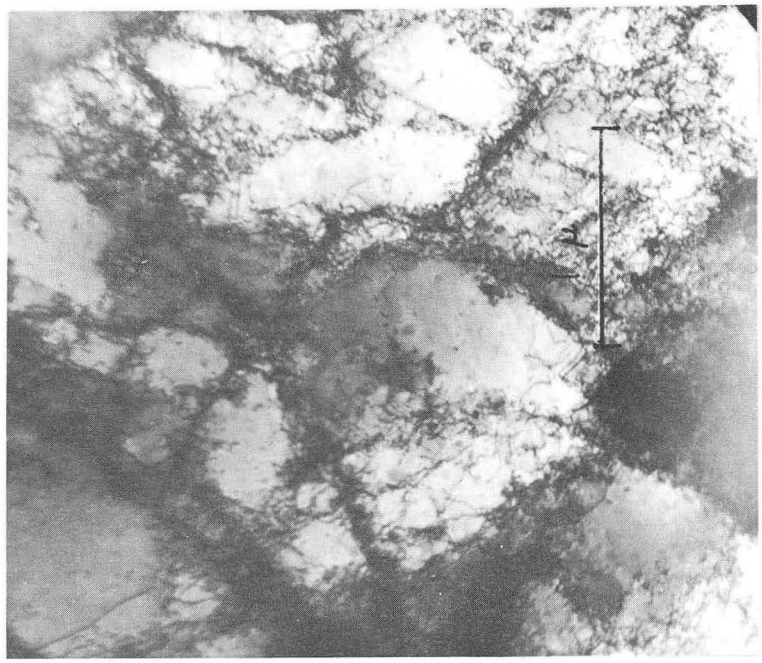

ZN-3905

Fig. 7

Fig. 6

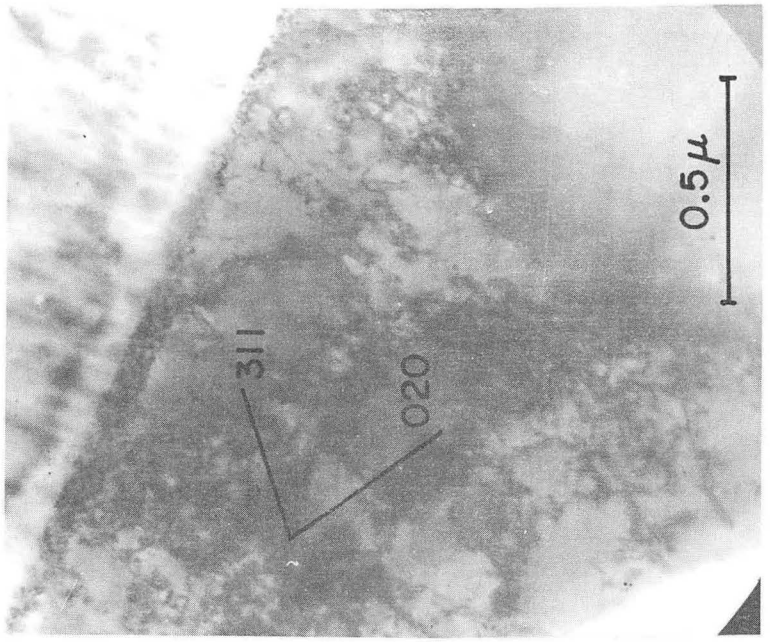

ZN-3906

Fig. 9

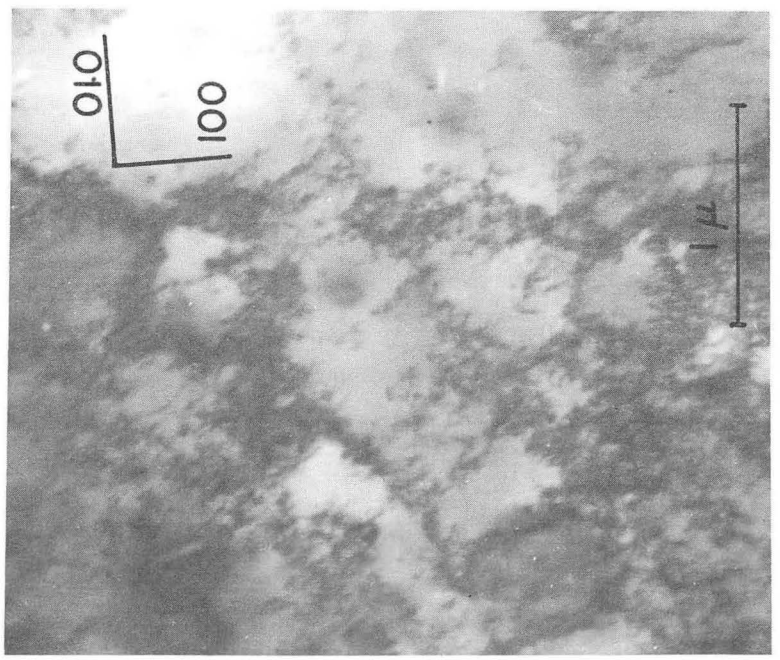

Fig. 8

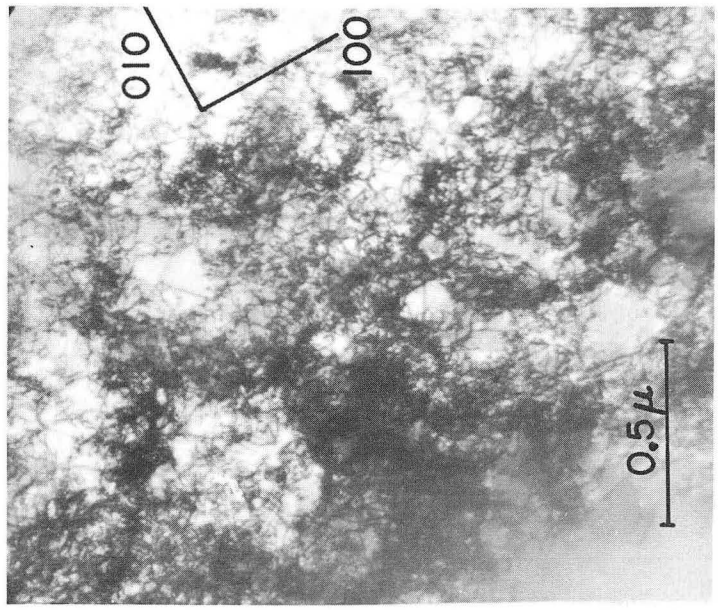

ZN-3907

Fig. 11

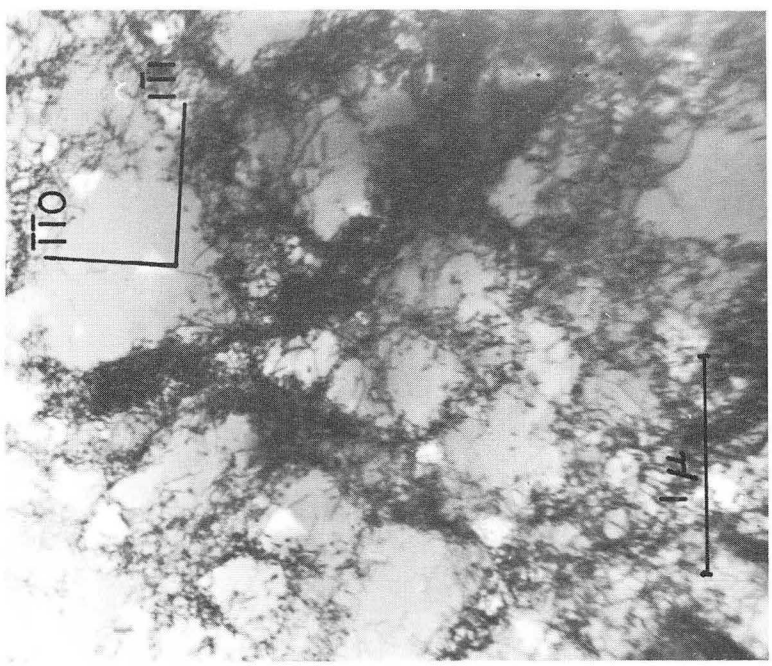

Fig. 10

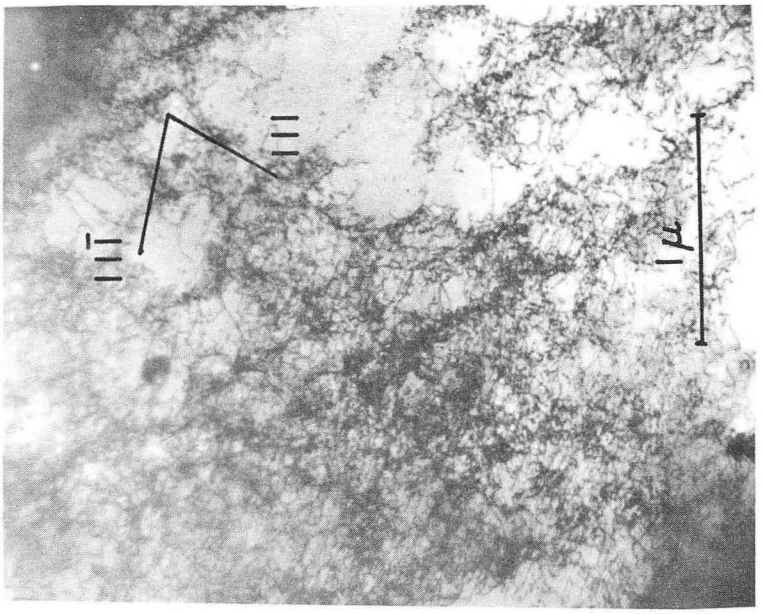

ZN-3908

Fig. 13

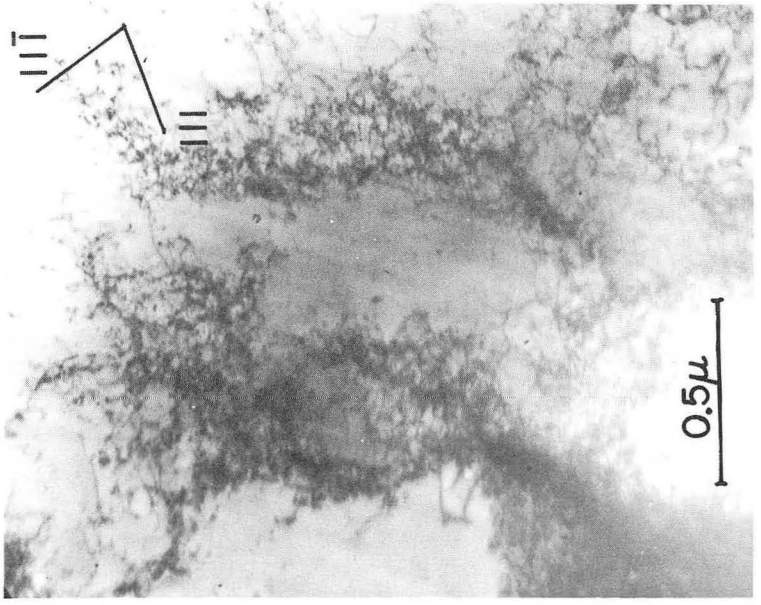

Fig. 12

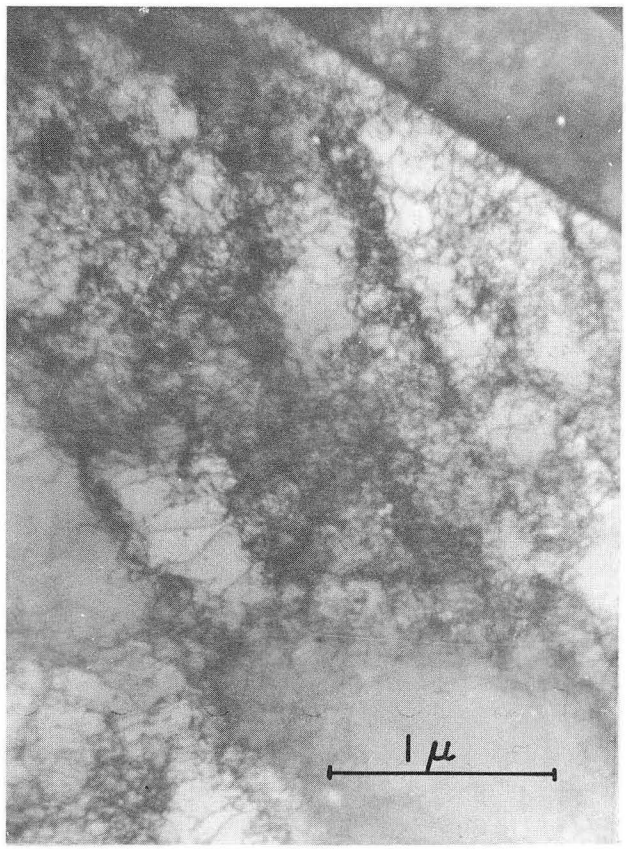

ZN-3909

Fig. 14

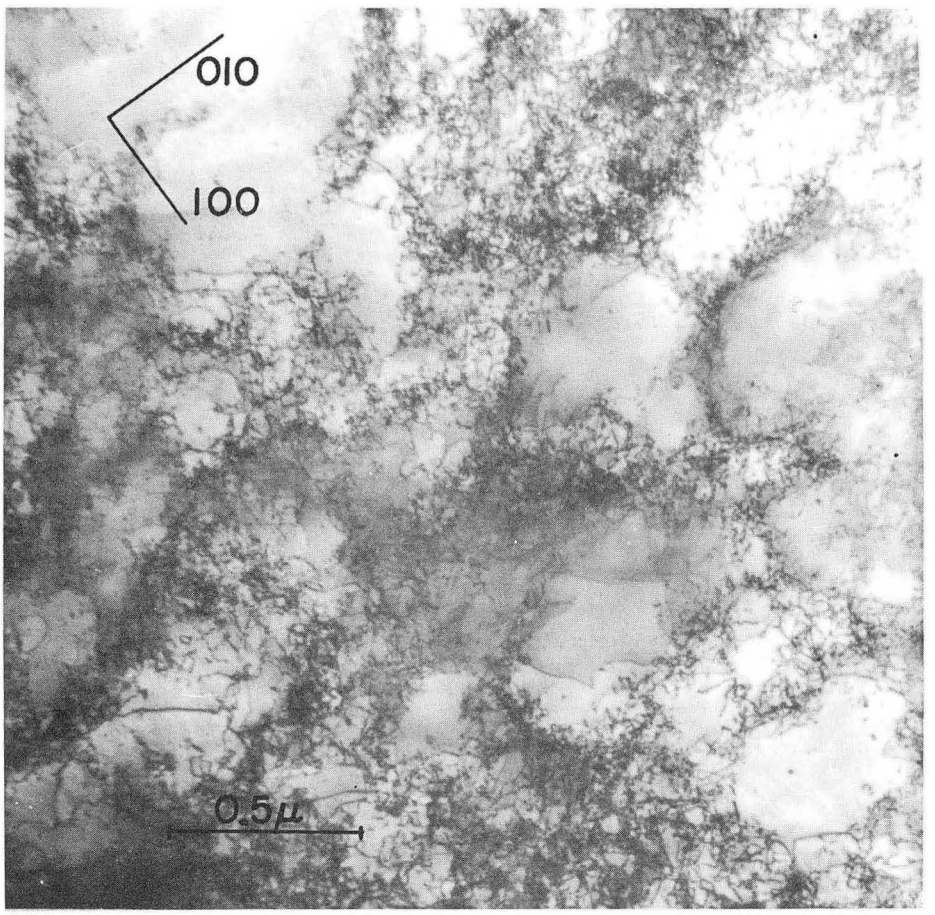

ZN-3910

Fig. 15

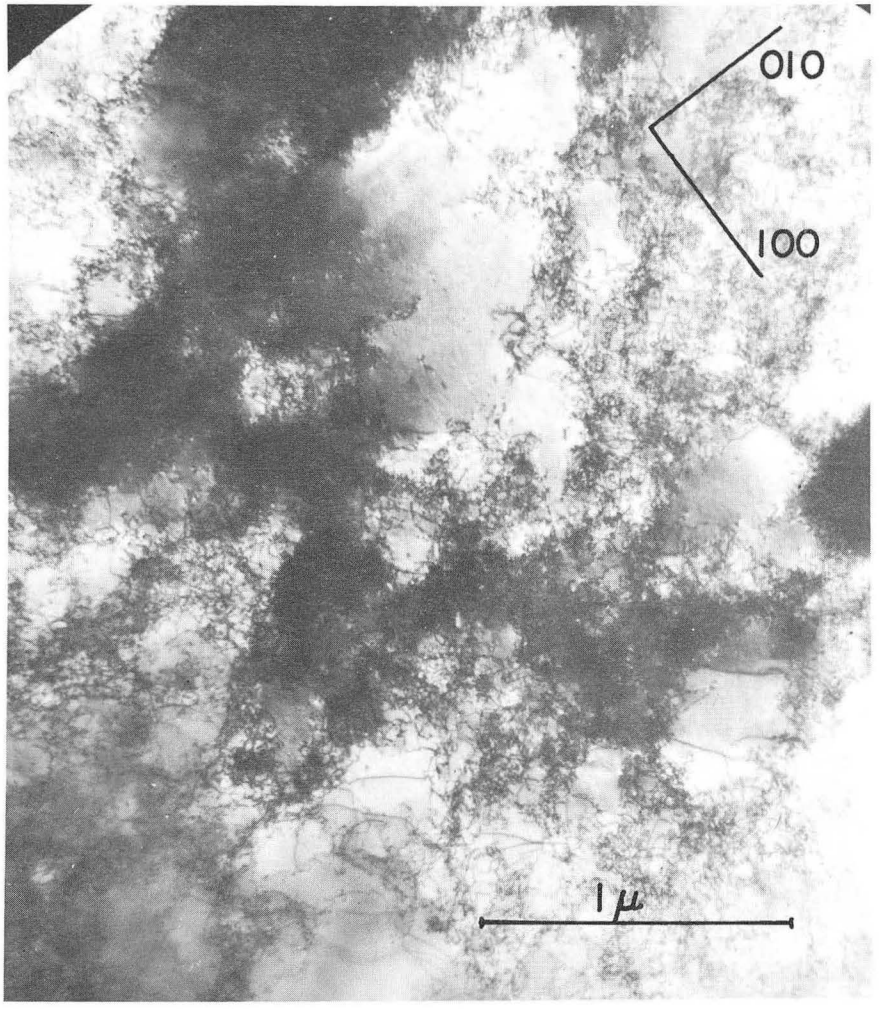

ZN-3911

Fig. 16

ZN-3912

Fig. 17

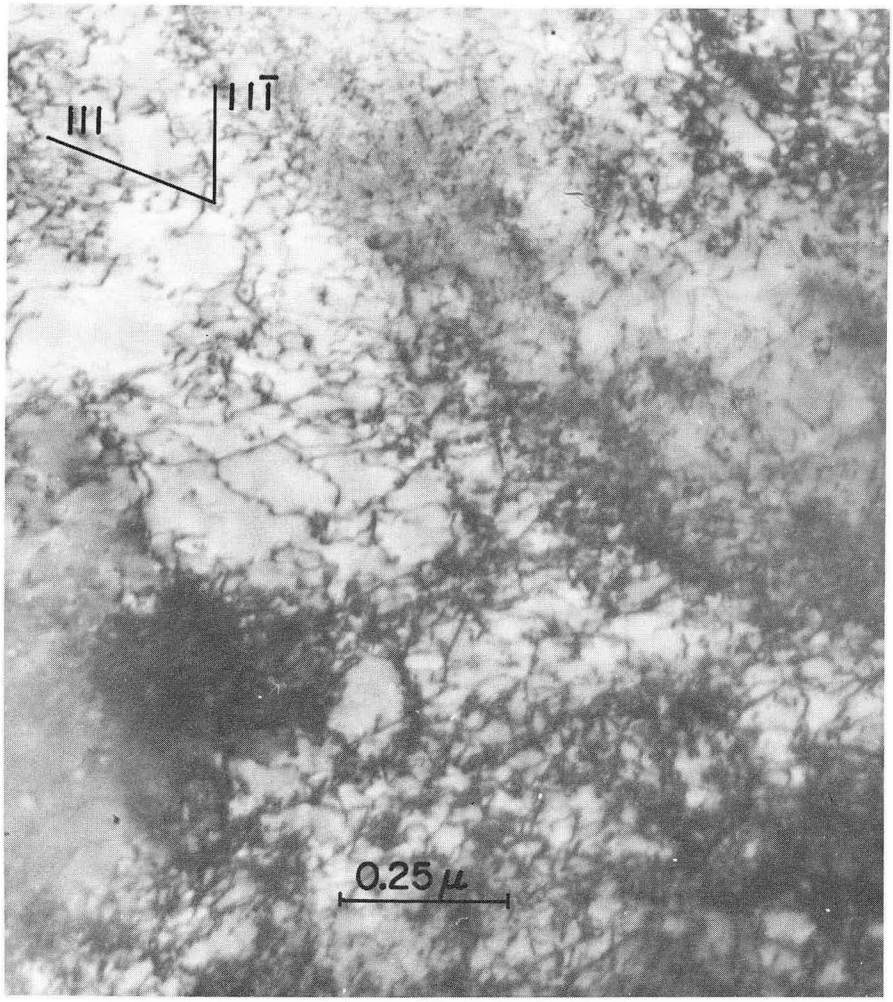

ZN-3913

Fig. 18

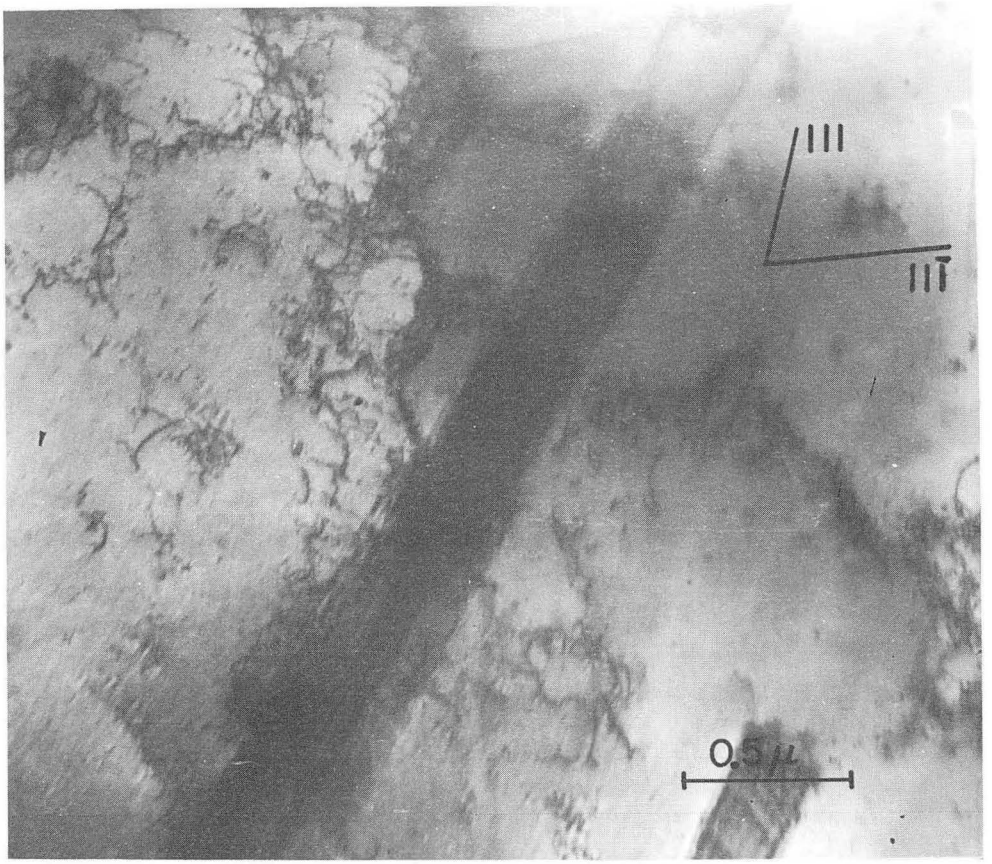

ZN-3914

Fig. 19

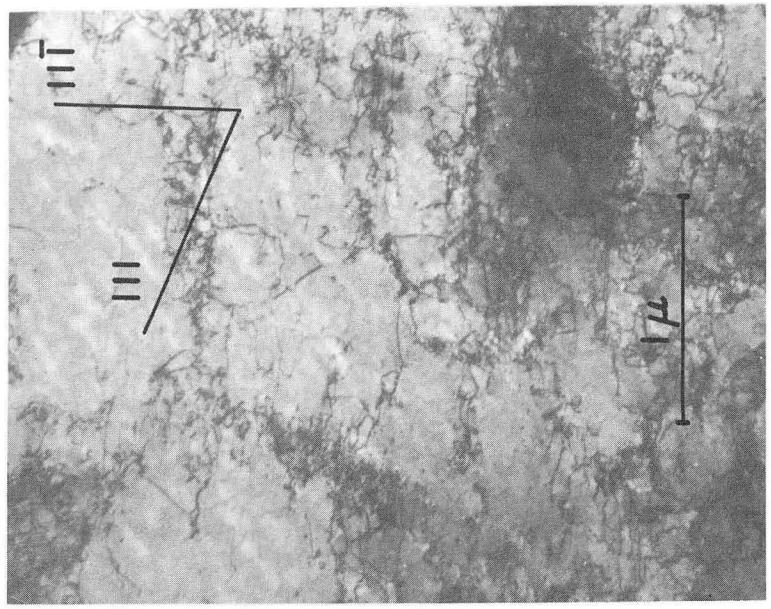

ZN-3915

Fig. 21

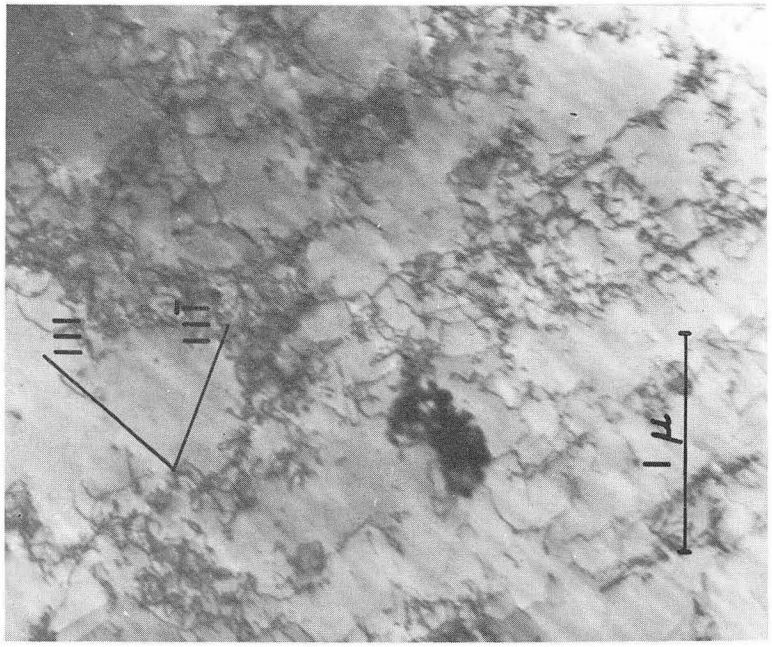

Fig. 20

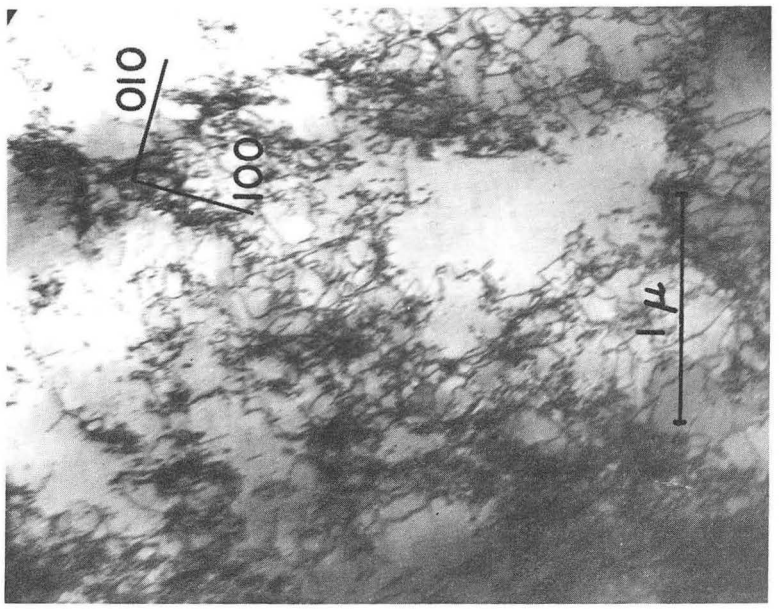

ZN-3916

Fig. 23

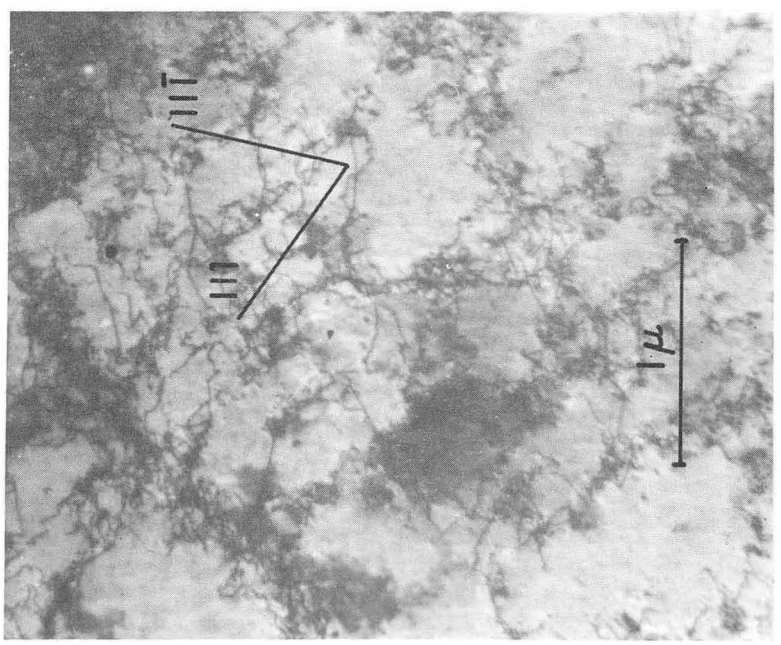

Fig. 22

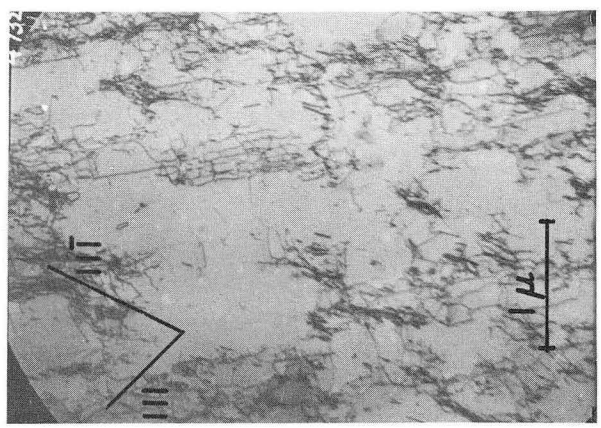

Fig. 24

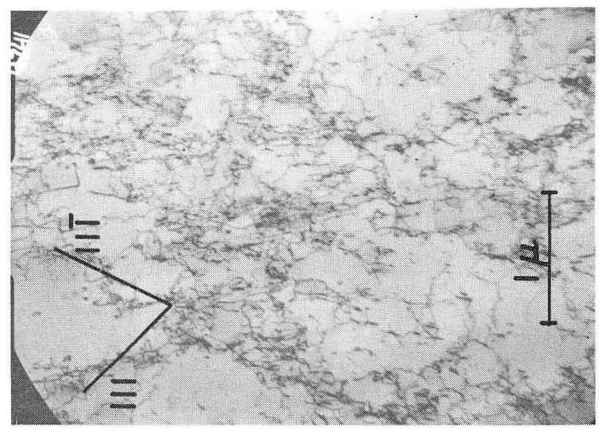

Fig. 25

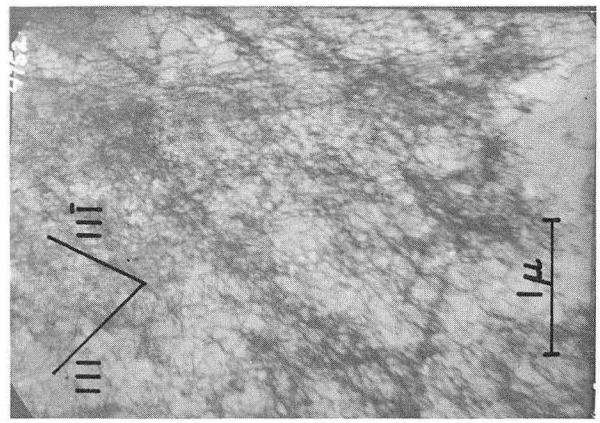

Fig. 26

ZN-3917

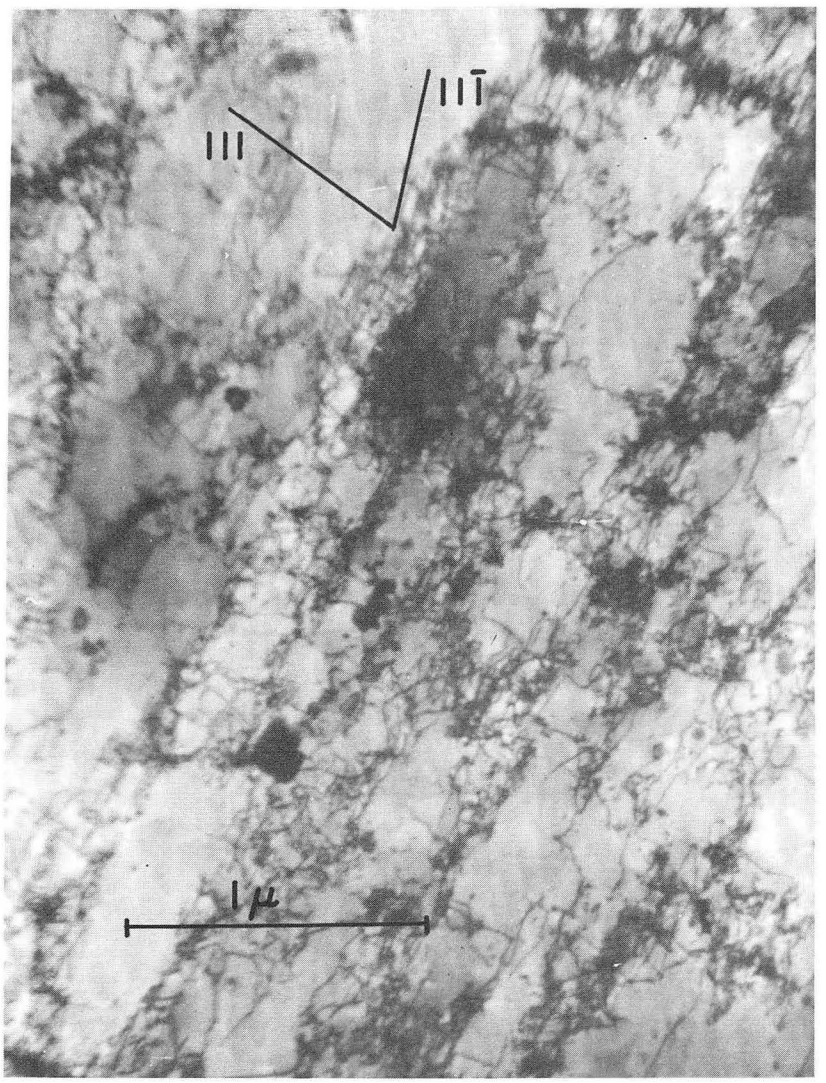

ZN-3918

Fig. 27

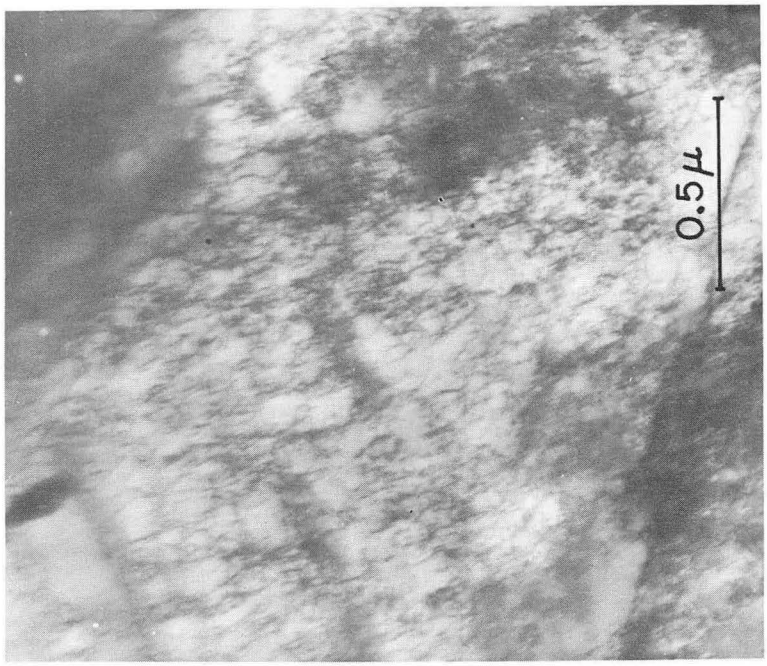

ZN-3919

Fig. 29

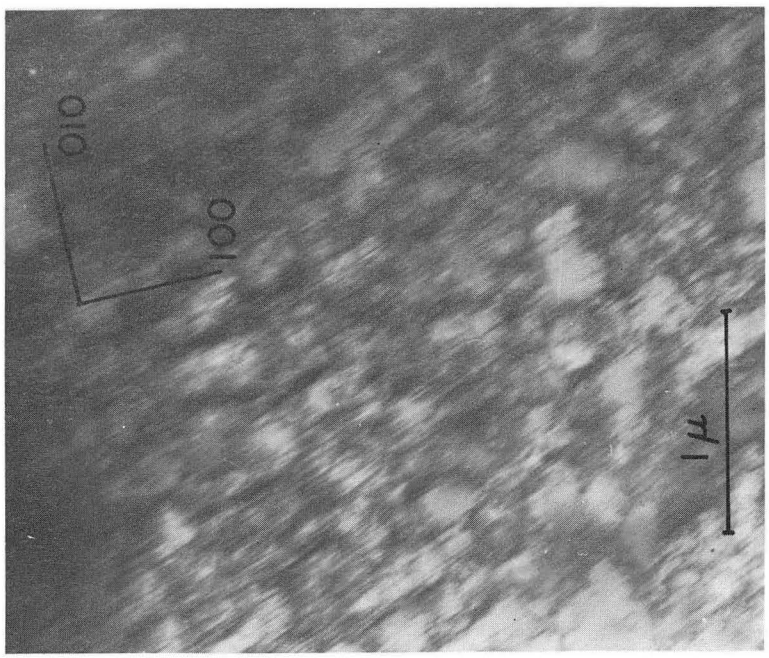

Fig. 28

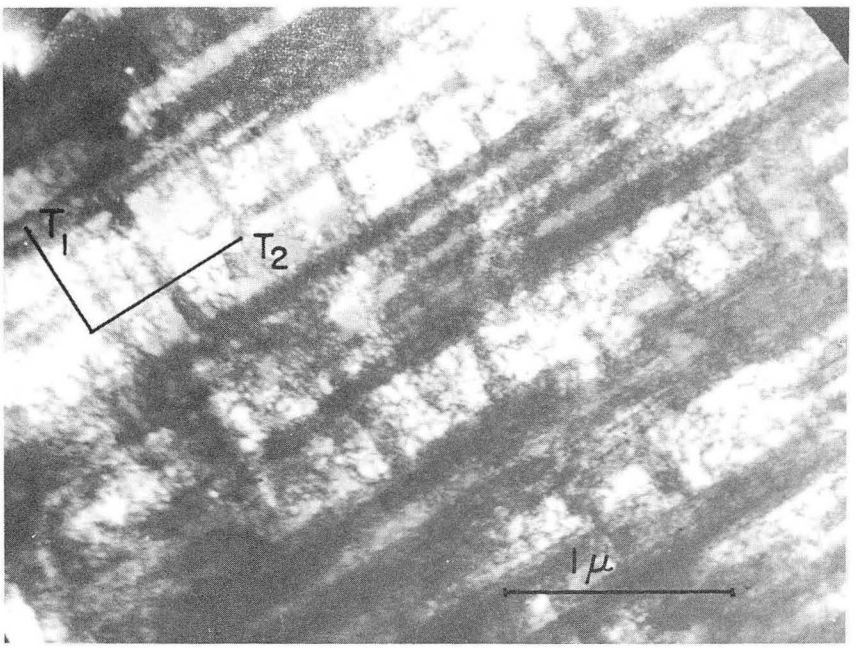

(a)

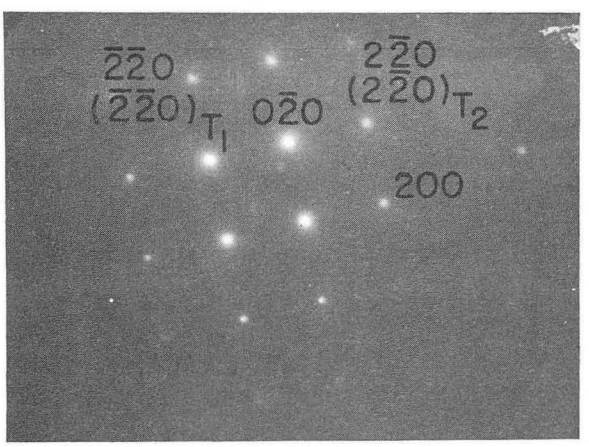

(b)

ZN-3920

Fig. 30

$\dot{6}\bar{6}0$ $(228)_{T_1}$ $(\bar{6}\bar{6}0)_{T_2}$	$\dot{6}\bar{4}0$	$\dot{6}\bar{2}0$	$\dot{6}00$ $(\bar{2}44)_{T_1}$ $(\bar{2}\bar{4}\bar{4})_{T_2}$	$\dot{6}20$	$\dot{6}40$	$\dot{6}60$ $(\bar{6}60)_{T_1}$ $(2\bar{2}\bar{8})_{T_2}$
$\dot{4}\bar{6}0$	$\dot{4}\bar{4}0$ $(\bar{4}\bar{4}0)_{T_2}$	$\dot{4}\bar{2}0$ $(024)_{T_1}$	$\dot{4}00$	$\dot{4}20$ $(0\bar{2}\bar{4})_{T_2}$	$\dot{4}40$ $(\bar{4}40)_{T_1}$	$\dot{4}60$
$\dot{2}\bar{6}0$	$\dot{2}\bar{4}0$ $(204)_{T_1}$	$\dot{2}\bar{2}0$ $(\bar{2}\bar{2}0)_{T_2}$	$\dot{2}00$	$\dot{2}20$ $(\bar{2}20)_{T_1}$	$\dot{2}40$ $(20\bar{4})_{T_2}$	$\dot{2}60$
$\dot{0}\bar{6}0$ $(4\bar{2}4)_{T_1}$ $(\bar{4}\bar{2}4)_{T_2}$	$\dot{0}\bar{4}0$	$\dot{0}\bar{2}0$	$\dot{0}$	$\dot{0}20$	$\dot{0}40$	$\dot{0}60$ $(\bar{4}2\bar{4})_{T_1}$ $(42\bar{4})_{T_2}$
$\dot{2}\bar{6}0$	$\dot{2}\bar{4}0$ $(\bar{2}04)_{T_2}$	$\dot{2}\bar{2}0$ $(2\bar{2}0)_{T_1}$	$\dot{2}00$	$\dot{2}20$ $(220)_{T_2}$	$\dot{2}40$ $(\bar{2}0\bar{4})_{T_1}$	$\dot{2}60$
$\dot{4}\bar{6}0$	$\dot{4}\bar{4}0$ $(4\bar{4}0)_{T_1}$	$\dot{4}\bar{2}0$ $(024)_{T_2}$	$\dot{4}00$	$\dot{4}20$ $(0\bar{2}\bar{4})_{T_1}$	$\dot{4}40$ $(440)_{T_2}$	$\dot{4}60$
$\dot{6}\bar{6}0$ $(6\bar{6}0)_{T_1}$ $(\bar{2}28)_{T_2}$	$\dot{6}\bar{4}0$	$\dot{6}\bar{2}0$	$\dot{6}00$ $(2\bar{4}\bar{4})_{T_1}$ $(244)_{T_2}$	$\dot{6}20$	$\dot{6}40$	$\dot{6}60$ $(\bar{2}\bar{2}\bar{8})_{T_1}$ $(660)_{T_2}$

MU-31440

Fig. 31

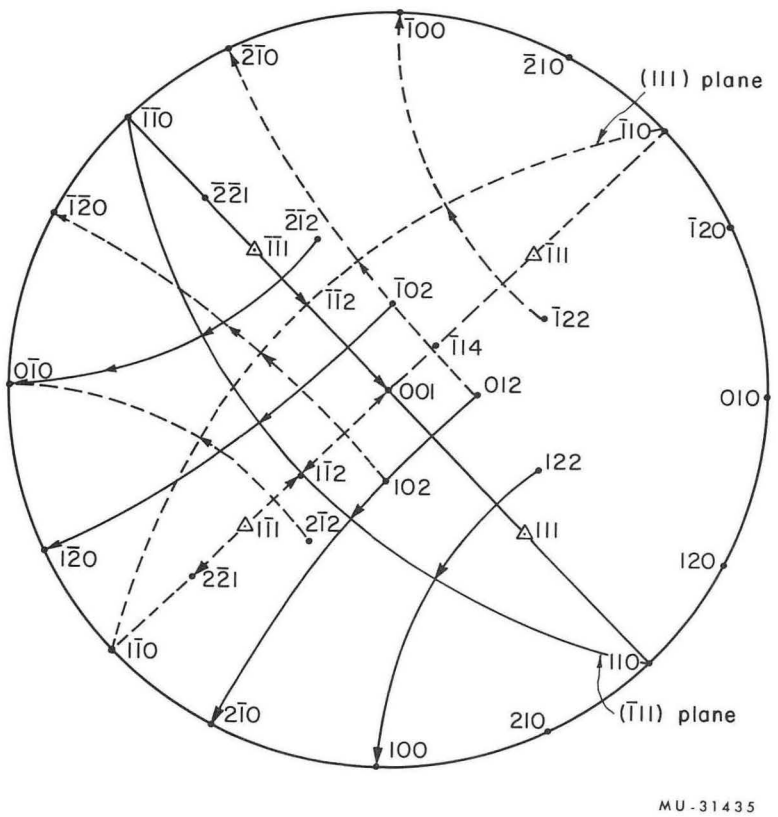
$\bar{1}00$
$\bar{2}\bar{1}0$
$\bar{2}10$
(111) plane
$\bar{1}\bar{1}0$
$\bar{1}10$
$\bar{2}\bar{2}1$
$\bar{1}\bar{2}0$
$\bar{2}\bar{1}2$
$\bar{1}20$
$\bar{1}\bar{1}1$
$\bar{1}11$
$\bar{1}\bar{1}2$
$\bar{1}02$
$\bar{1}22$
$\bar{1}14$
$0\bar{1}0$
001
012
010
122
$1\bar{1}2$
102
$\bar{1}\bar{1}1$
$2\bar{1}2$
111
$\bar{1}\bar{2}0$
120
$2\bar{2}1$
$1\bar{1}0$
110
$2\bar{1}0$
210
($\bar{1}$11) plane
100
MU-31435

Fig. 32

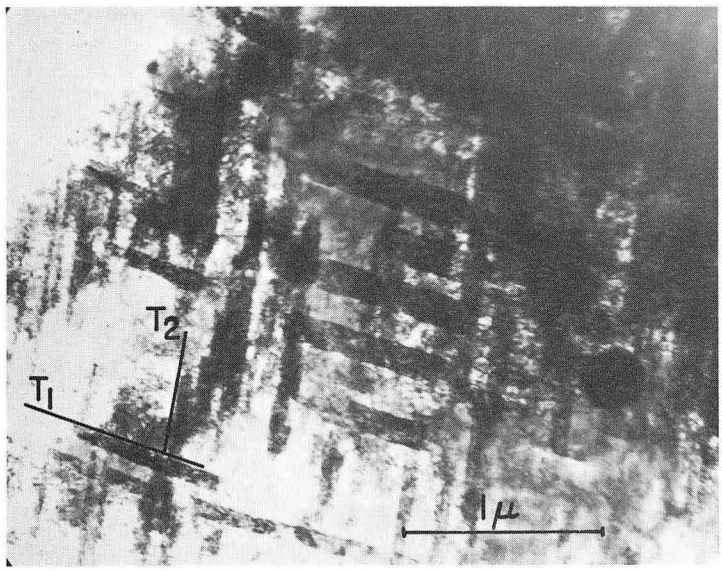

(a)

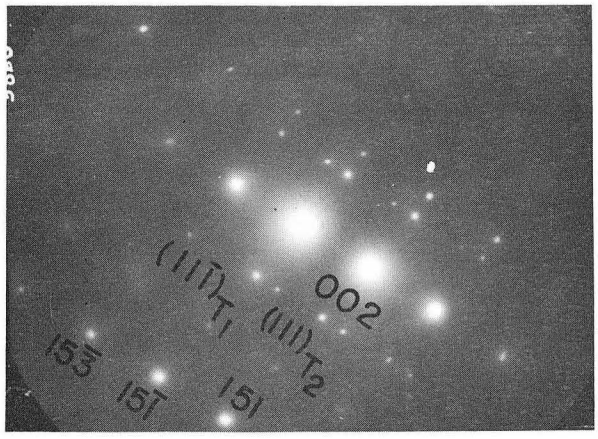

(b)

ZN-3921

Fig. 33

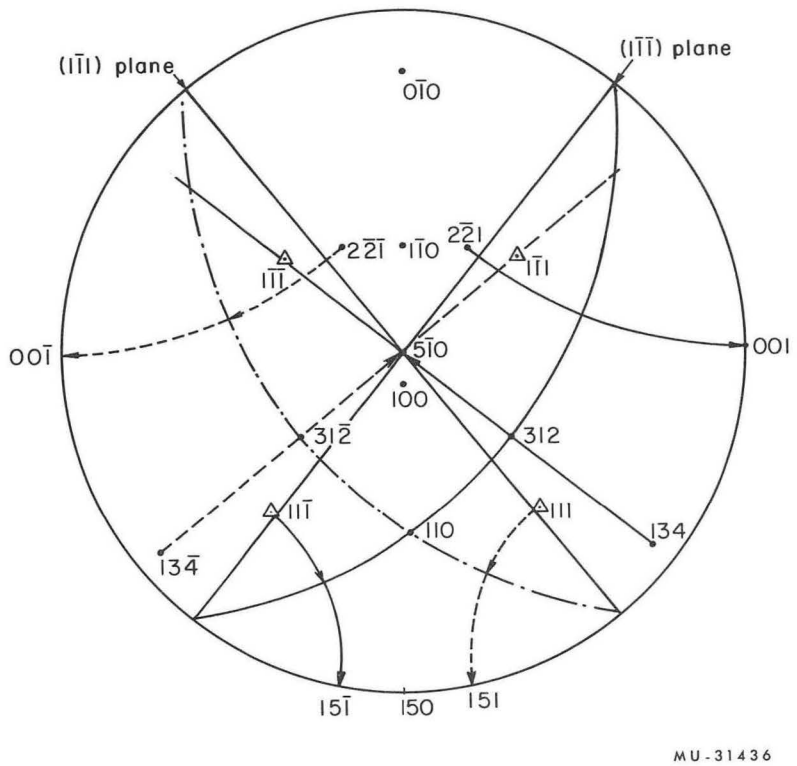
(1$\bar{1}$1) plane
(1$\bar{1}\bar{1}$) plane
0$\bar{1}$0
2$\bar{2}$1
1$\bar{1}$0
2$\bar{2}$1
1$\bar{1}$1
1$\bar{1}$1
00$\bar{1}$
001
5$\bar{1}$0
100
31$\bar{2}$
312
11$\bar{1}$
111
110
134
13$\bar{4}$
15$\bar{1}$
150
151
MU-31436

Fig. 34

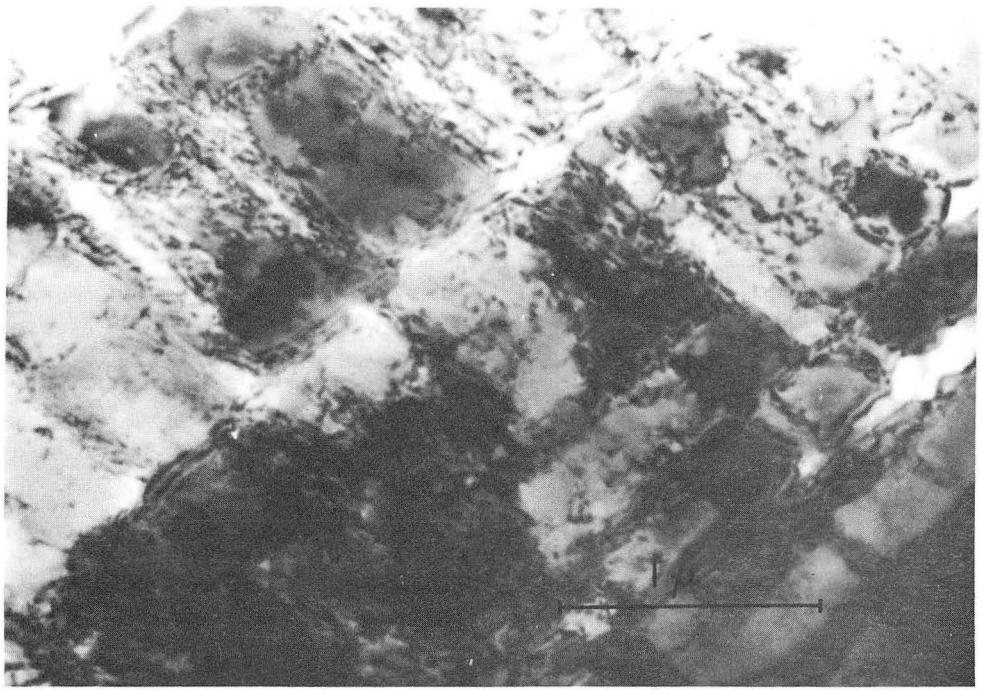

(a)

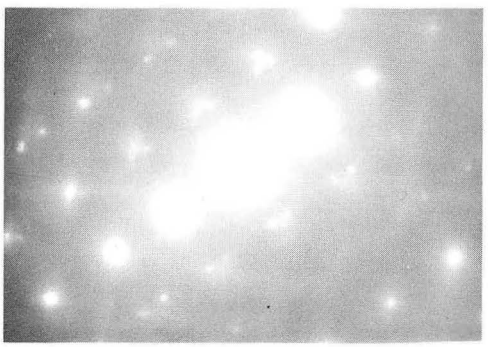

(b)

ZN-3922

Fig. 35

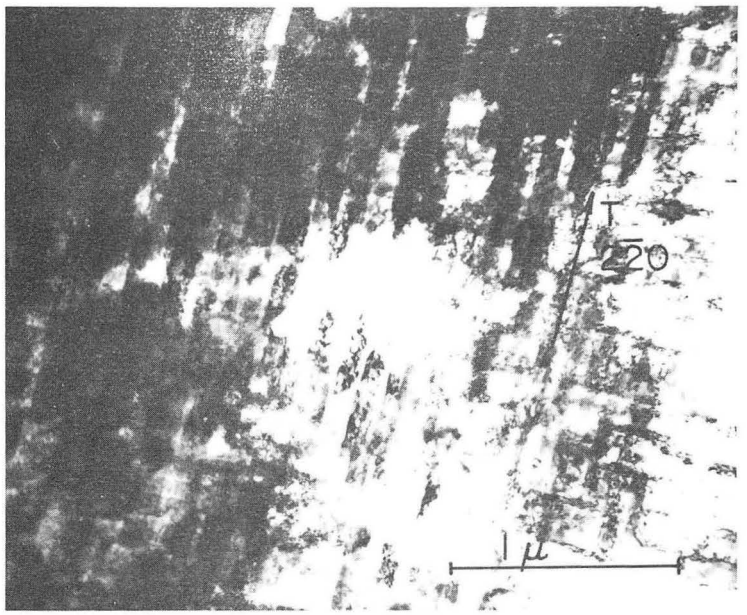

(a)

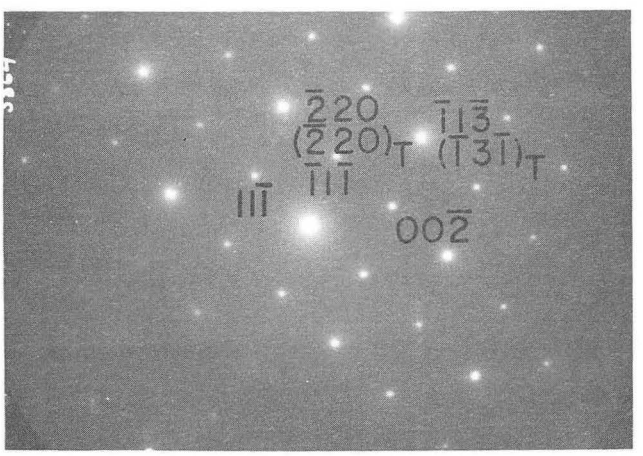

(b)

ZN-3923

Fig. 36

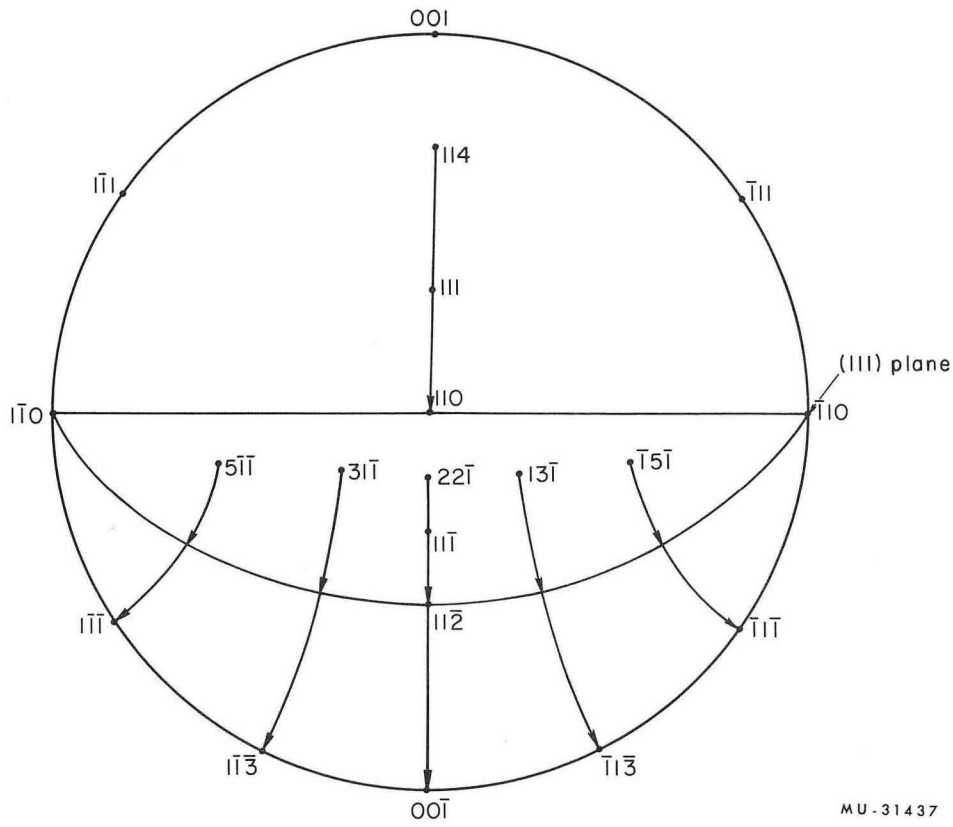
001
114
$1\bar{1}1$
$\bar{1}11$
111
(111) plane
$1\bar{1}0$
110
$\bar{1}10$
$5\bar{1}\bar{1}$
$31\bar{1}$
$22\bar{1}$
$13\bar{1}$
$\bar{1}5\bar{1}$
$11\bar{1}$
$1\bar{1}\bar{1}$
$11\bar{2}$
$\bar{1}1\bar{1}$
$1\bar{1}\bar{3}$
$\bar{1}1\bar{3}$
$00\bar{1}$
MU-31437

Fig. 37

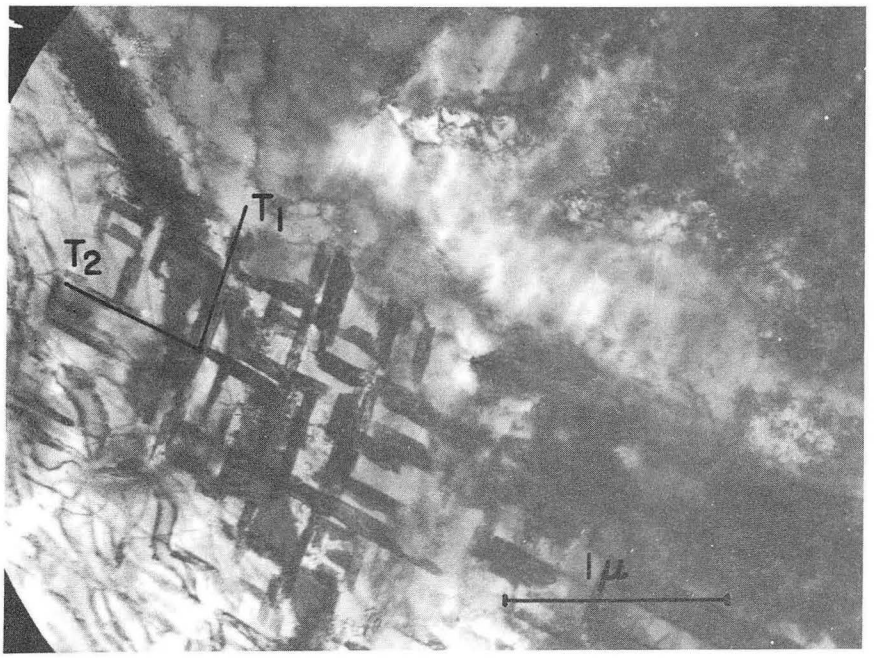

(a)

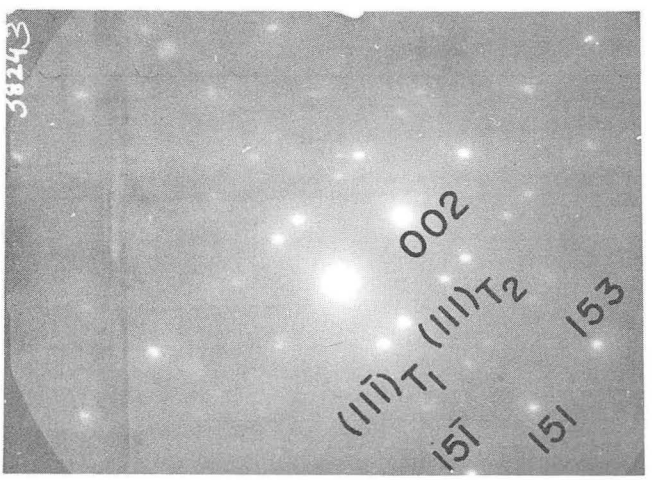

(b)

ZN-3924

Fig. 38

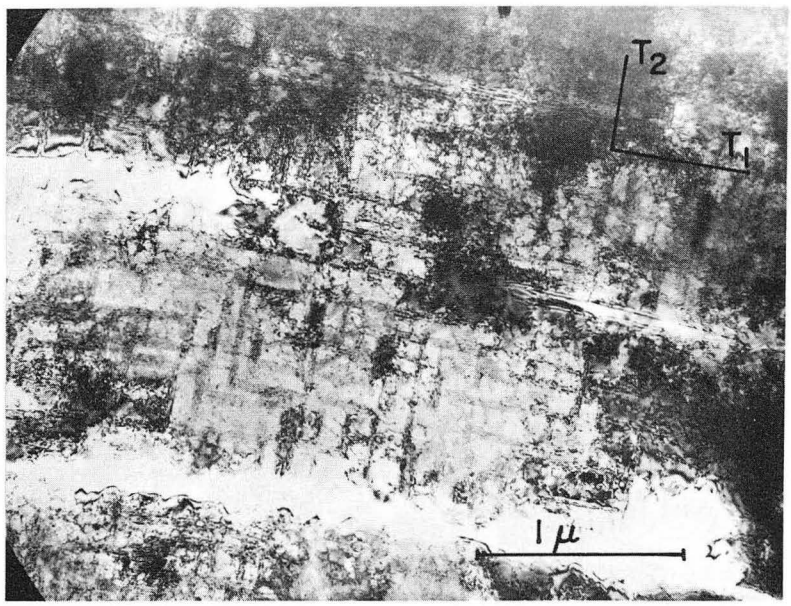

(a)

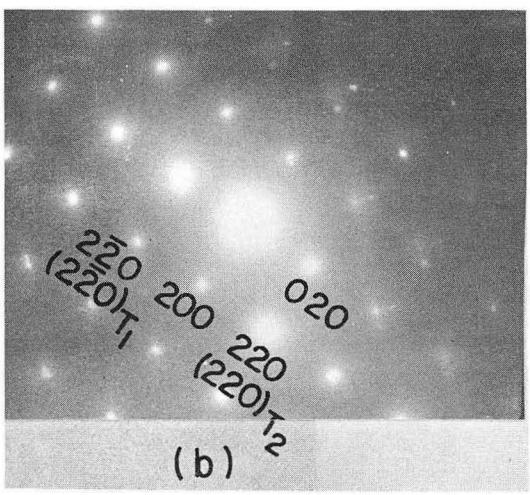

(b)

ZN-3925

Fig. 39

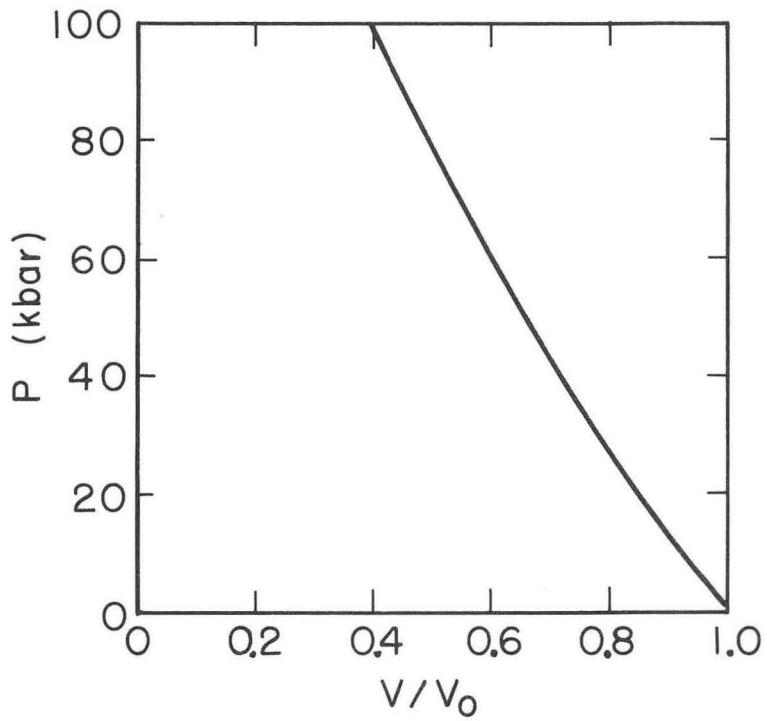

MU-31438

Fig. 40

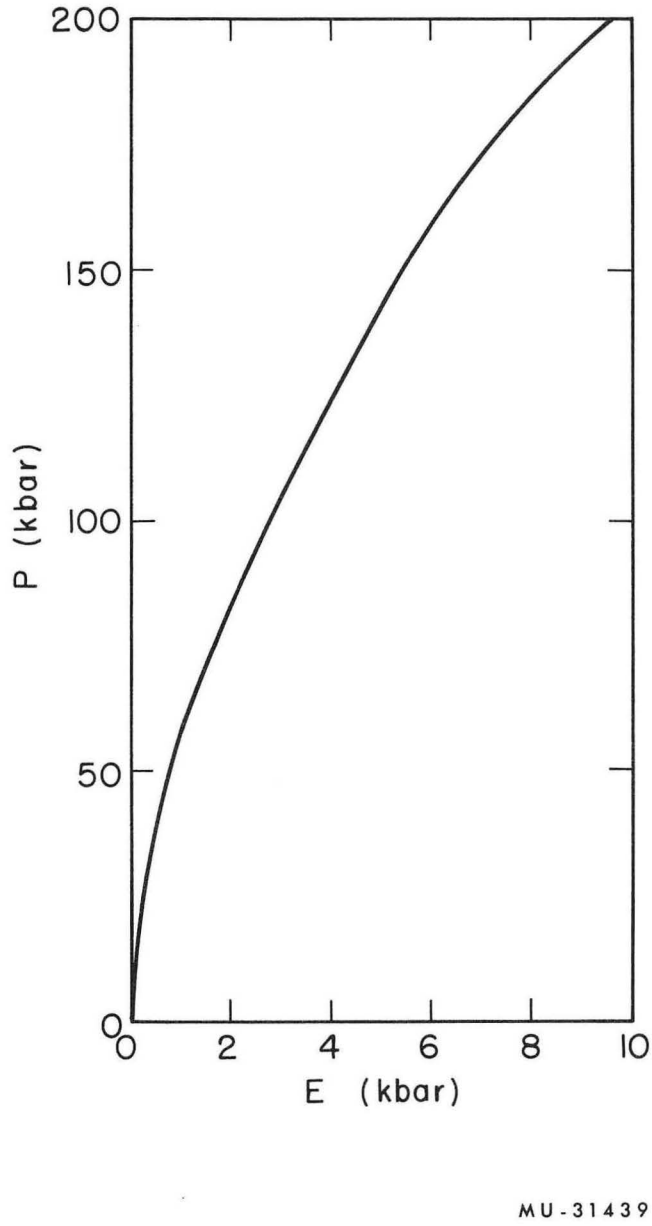

Fig. 41

This report was prepared as an account of Government sponsored work. Neither the United States, nor the Commission, nor any person acting on behalf of the Commission:

A. Makes any warranty or representation, expressed or implied, with respect to the accuracy, completeness, or usefulness of the information contained in this report, or that the use of any information, apparatus, method, or process disclosed in this report may not infringe privately owned rights; or

B. Assumes any liabilities with respect to the use of, or for damages resulting from the use of any information, apparatus, method, or process disclosed in this report.

As used in the above, "person acting on behalf of the Commission" includes any employee or contractor of the Commission, or employee of such contractor, to the extent that such employee or contractor of the Commission, or employee of such contractor prepares, disseminates, or provides access to, any information pursuant to his employment or contract with the Commission, or his employment with such contractor.